Supporting Information

Photoreduction of Carbon Dioxide Enhanced by Cu Atoms Doped within the Pd Cluster Supported on TiO_2: Mechanism, Selectivity, and Catalytic Descriptor

Jia-Jia Yang[1*], Shi-Ru Zhang[2], Feng Li[1], Laicai Li[1], Wei-Hai Fang[2], and Ganglong Cui[2*]

[1]College of Chemistry and Material Science, Sichuan Normal University, Chengdu 610068, China and [2]Key Laboratory of Theoretical and Computational Photochemistry, Ministry of Education, College of Chemistry, Beijing Normal University, Beijing 100875, China

*E-mail: jiajiayang@sicnu.edu.cn; ganglong.cui@bnu.edu.cn

Contents

Figures

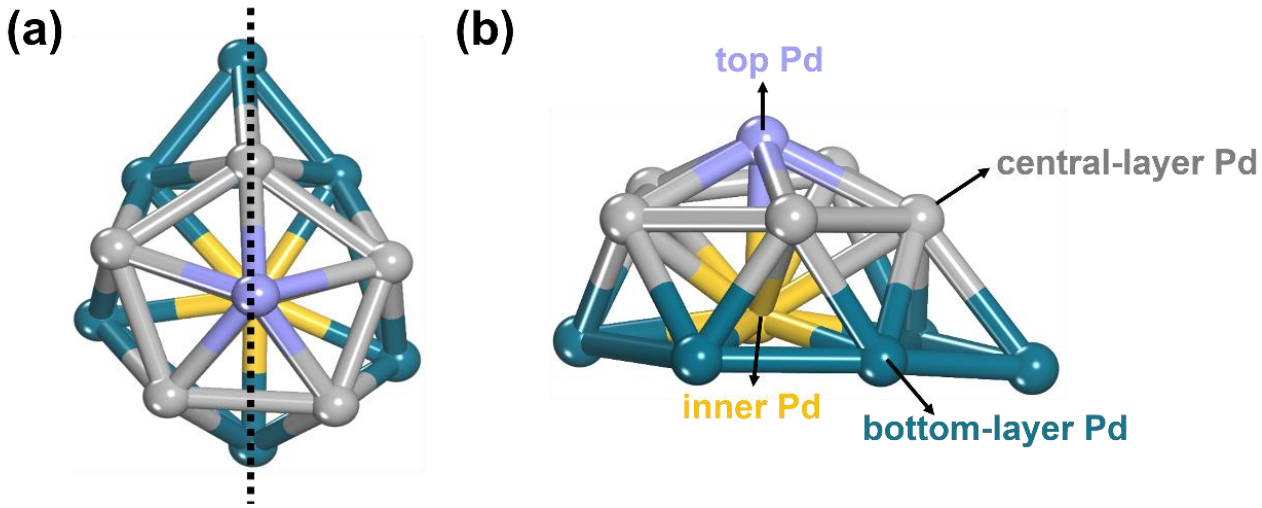

Figure S1. (a) The structure and (b) related classification of Pd atoms in the Pd_{13} nanocluster supported on the TiO_2(101) surface. The top layer has one Pd atom (purple), the central layer has five Pd atoms (gray), the inner layer has one Pd atom (yellow), and the bottom layer has six Pd atoms (cyan).

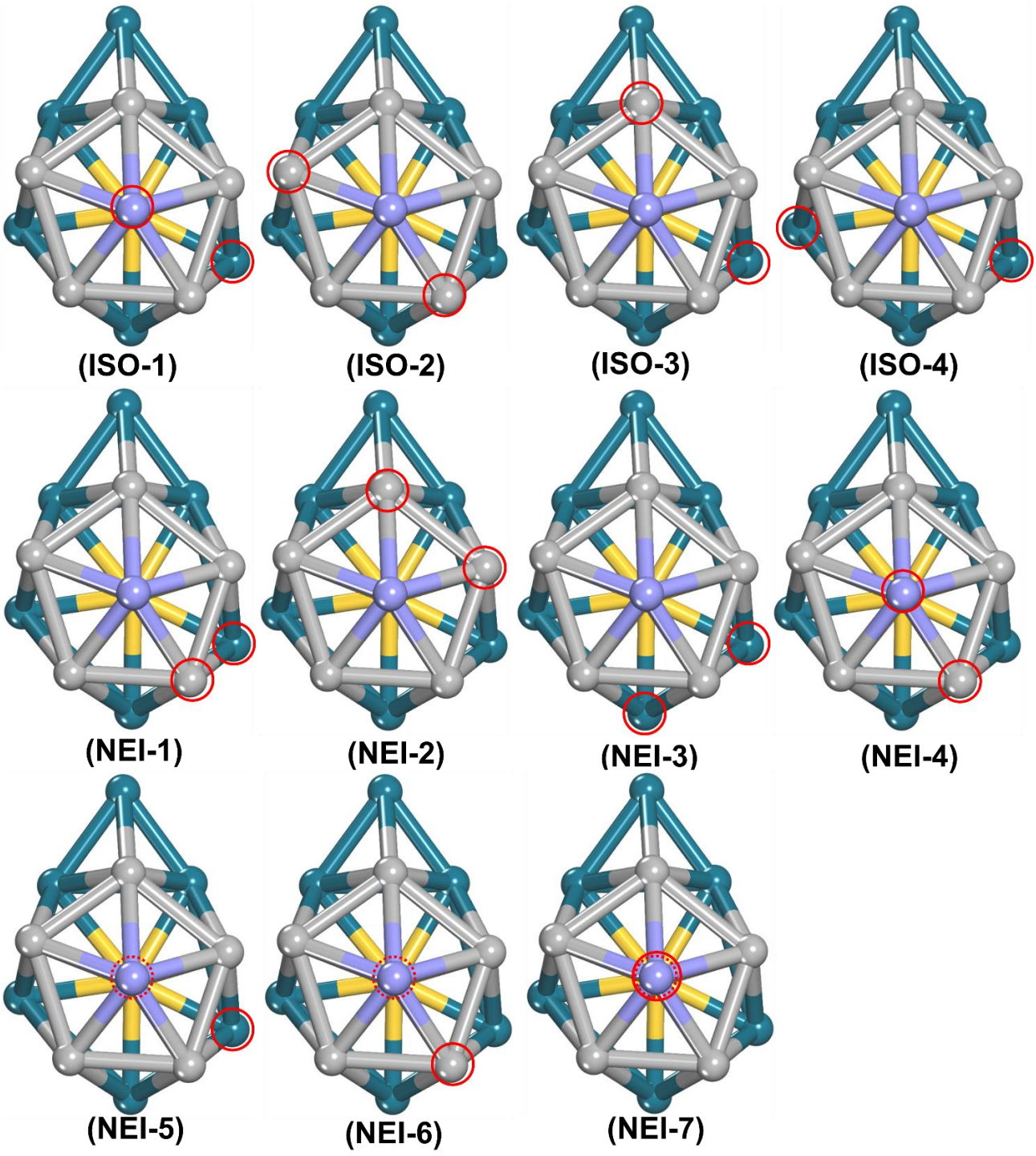

Figure S2. The location of the two Cu atoms (red circles) within the Pd_{13} nanocluster. For ISO-1 to ISO-4, the two Cu atoms are isolated spatially without any Cu-Cu bond formed; while, for NEI-1 to NEI-7, the two Cu atoms are spatially close to each other forming a Cu-Cu bond.

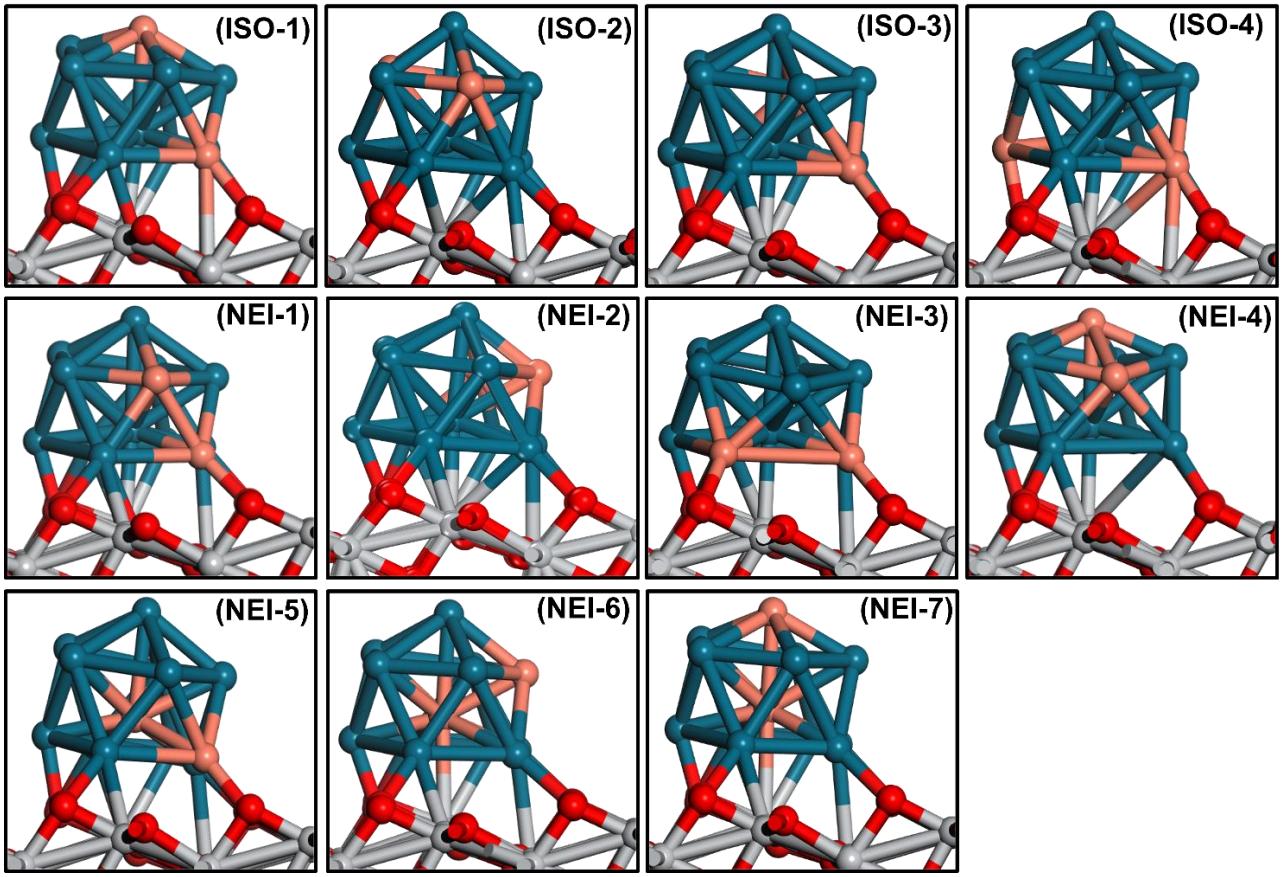

Figure S3. The eleven interface models of $Pd_{11}Cu_2@TiO_2$ with the two Cu atoms located at the different positions of Pd_{13}. For ISO-1 to ISO-4, the two Cu atoms are isolated spatially, and for NEI-1 to NEI-7, the two Cu atoms are spatially close to each other forming a Cu-Cu bond.

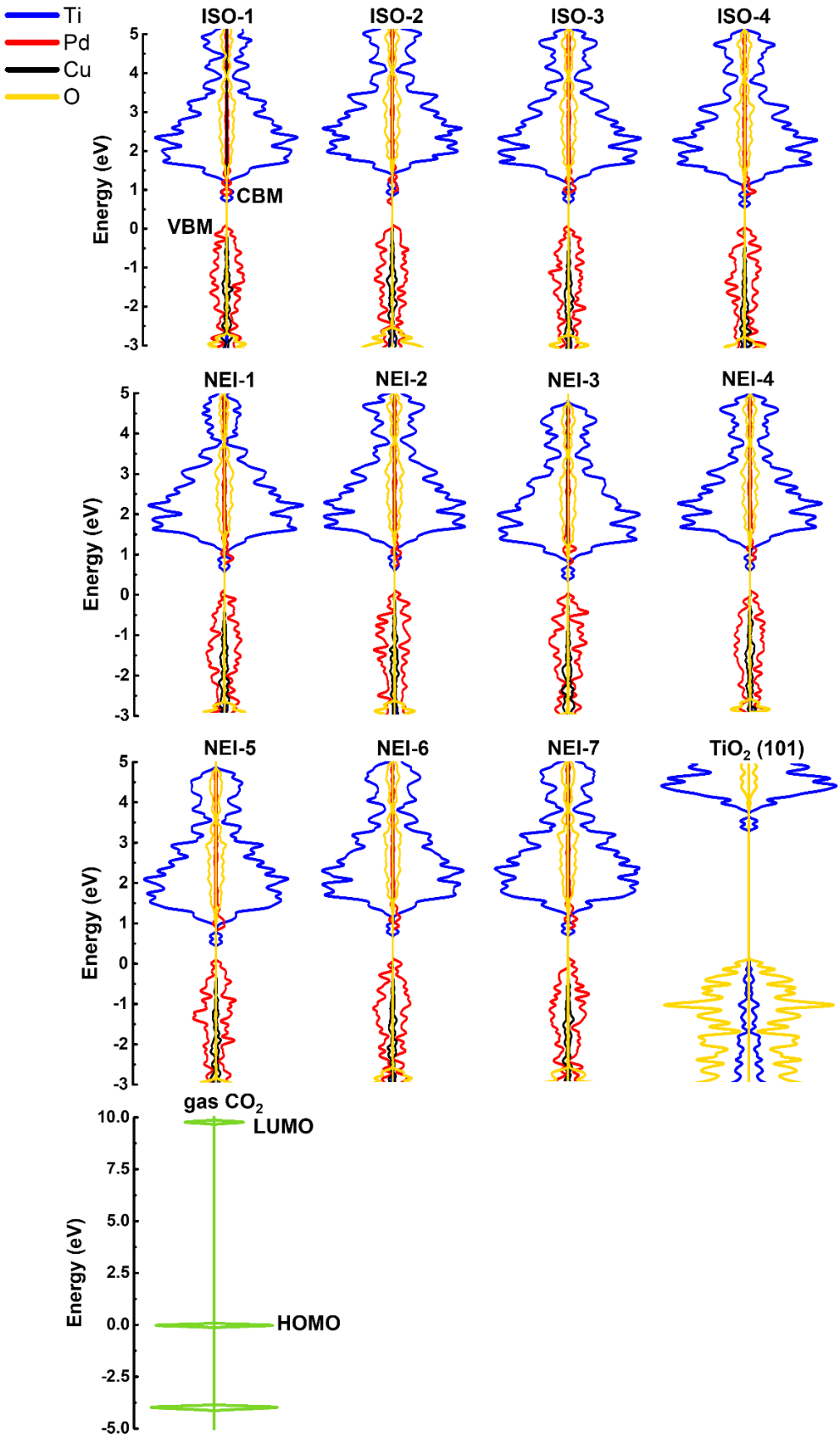

Figure S4. The DOSs of the eleven models of $Pd_{11}Cu_2$@TiO_2(101), TiO_2(101), and CO_2 gas. The Fermi level is set to the zero point.

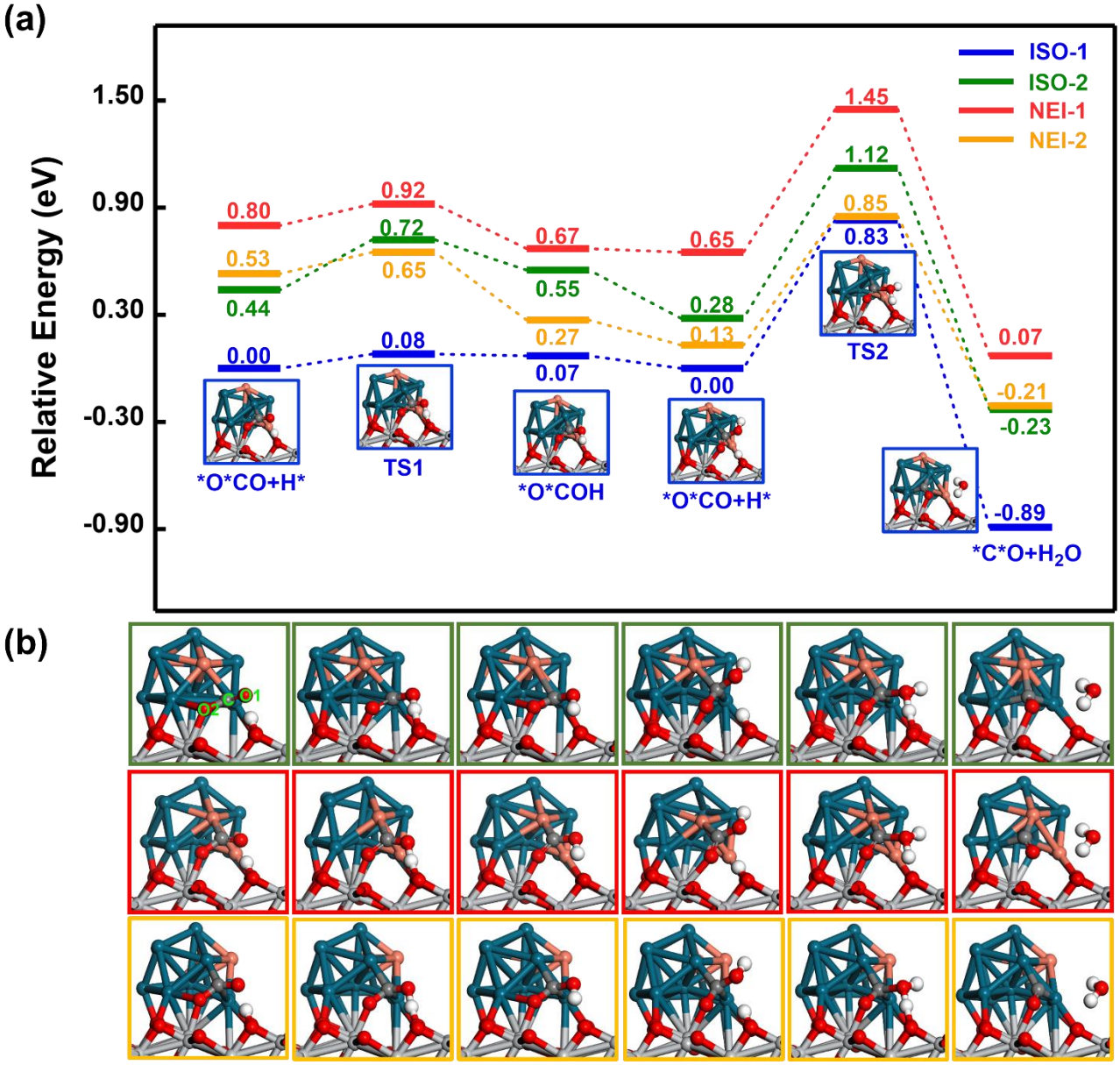

Figure S5. (a) The reaction pathways for *O*CO to *C*O related to the four interface models (ISO-1, ISO-2, NEI-1, and NEI-2) of $Pd_{11}Cu_2@TiO_2$, in which O1 of *O*CO is consecutively hydrogenated, followed by a dehydration reaction. Relevant transition states and intermediates related to these four models are also shown in panels a (ISO-1) and b (ISO-2, NEI-1, and NEI-2). Ti, O, Pd, Cu, C, and H atoms are in gray, red, cyan, orange, dark grey, and white, respectively.

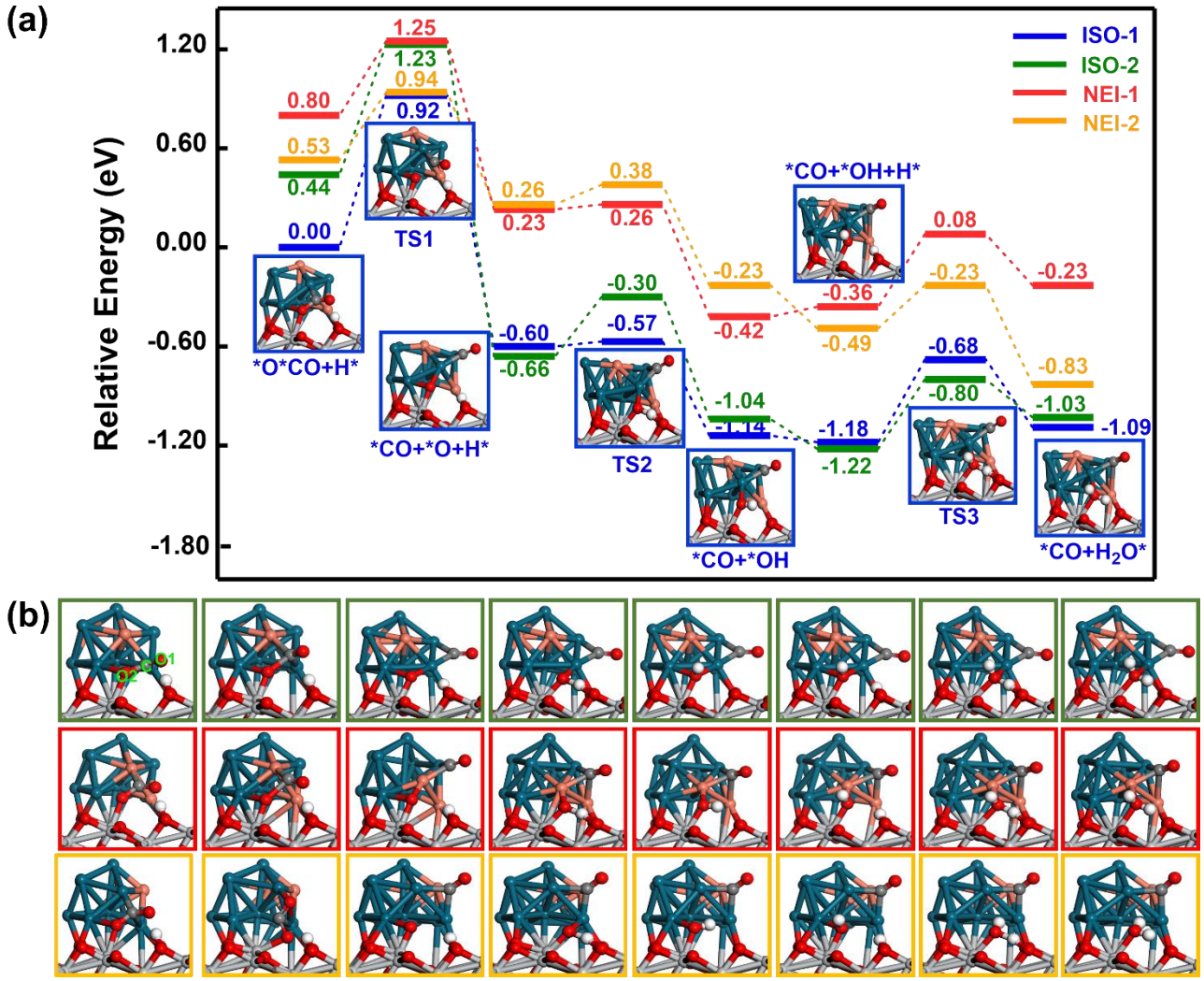

Figure S6. (a) The reaction pathways for *O*CO to *CO related to the four interface models (ISO-1, ISO-2, NEI-1, and NEI-2) of $Pd_{11}Cu_2$@TiO_2, in which *CO_2 dissociates its C-O2 bond and O2* is hydrogenated to H_2O. Relevant transition states and intermediates related to these four models are also shown in panels a (ISO-1) and b (ISO-2, NEI-1, and NEI-2). Ti, O, Pd, Cu, C, and H atoms are in gray, red, cyan, orange, dark grey, and white, respectively.

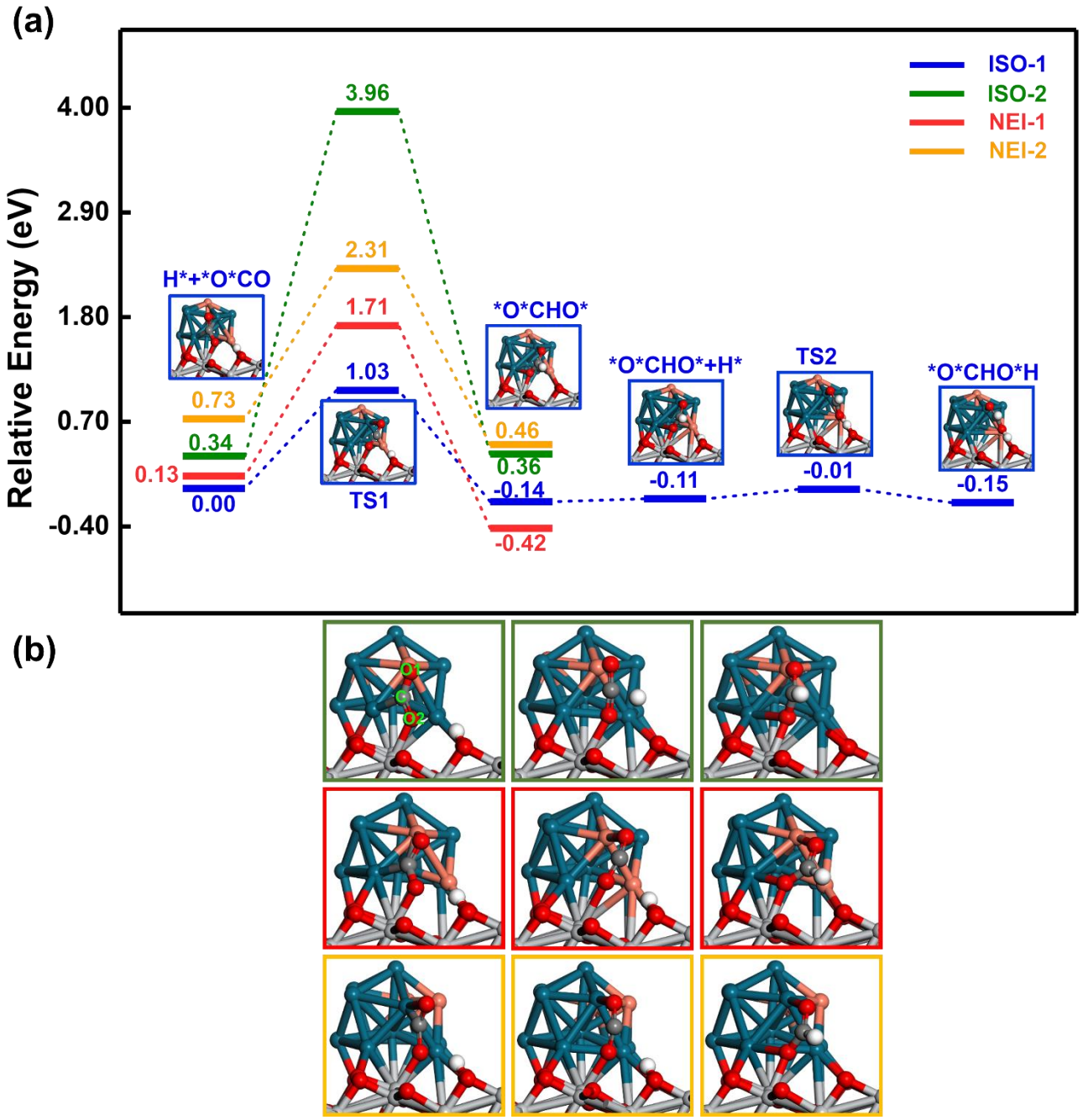

Figure S7. (a) The reaction pathways for *O*CO to CH*OOH (or *OCHO*) related to the four interface models (ISO-1, ISO-2, NEI-1, and NEI-2) of $Pd_{11}Cu_2$@TiO_2. Relevant transition states and intermediates related to these four models are also shown in panels a (ISO-1) and b (ISO-2, NEI-1, and NEI-2). Ti, O, Pd, Cu, C, and H atoms are in gray, red, cyan, orange, dark grey, and white, respectively.

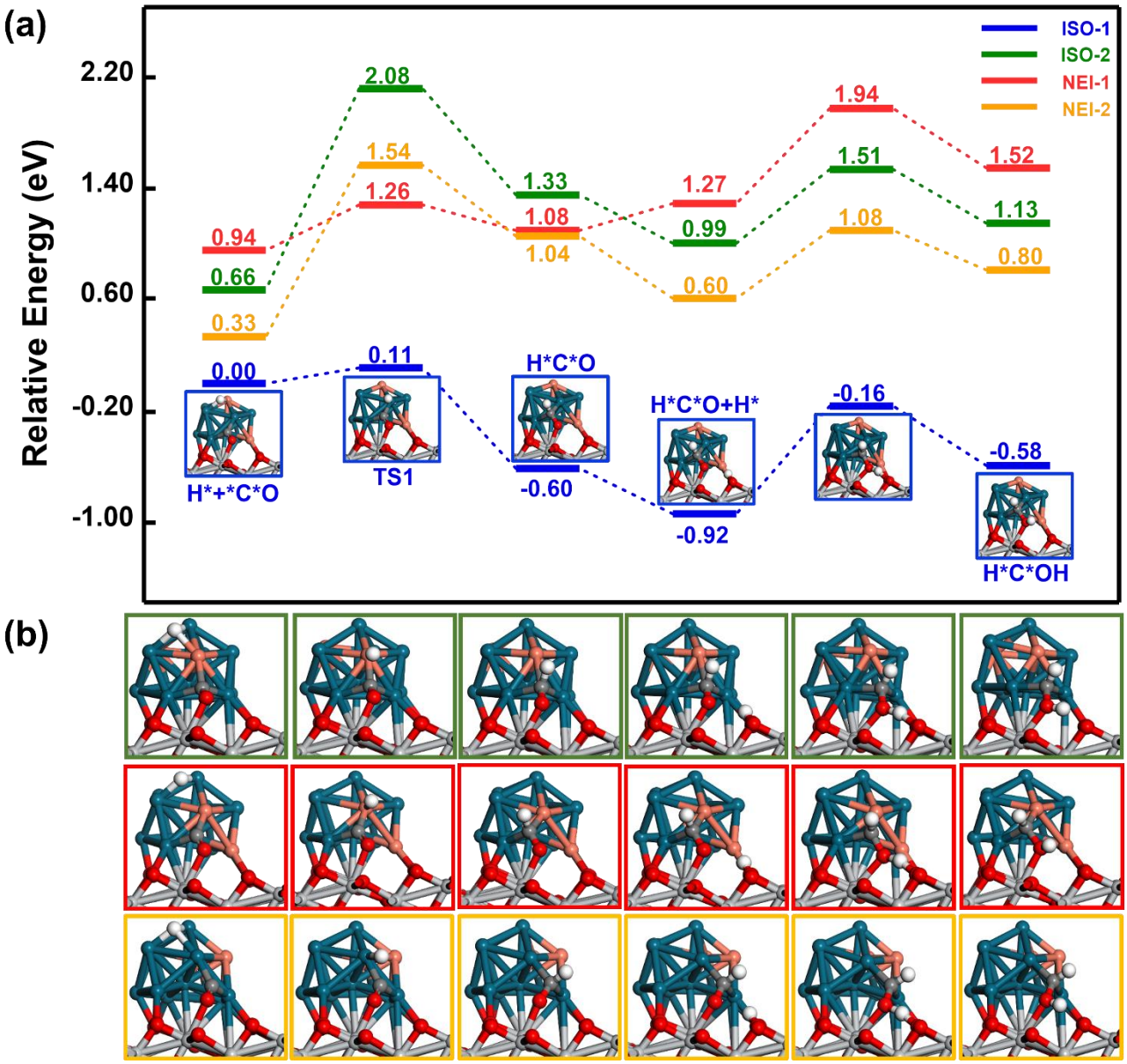

Figure S8. (a) The reaction pathways for *C*O to H*C*OH related to the four interface models (ISO-1, ISO-2, NEI-1, and NEI-2) of $Pd_{11}Cu_2$@TiO_2, in which *C and *O are hydrogenated sequentially. Relevant transition states and intermediates related to these four models are also shown in panels a (ISO-1) and b (ISO-2, NEI-1, and NEI-2). Ti, O, Pd, Cu, C, and H atoms are in gray, red, cyan, orange, dark grey, and white, respectively.

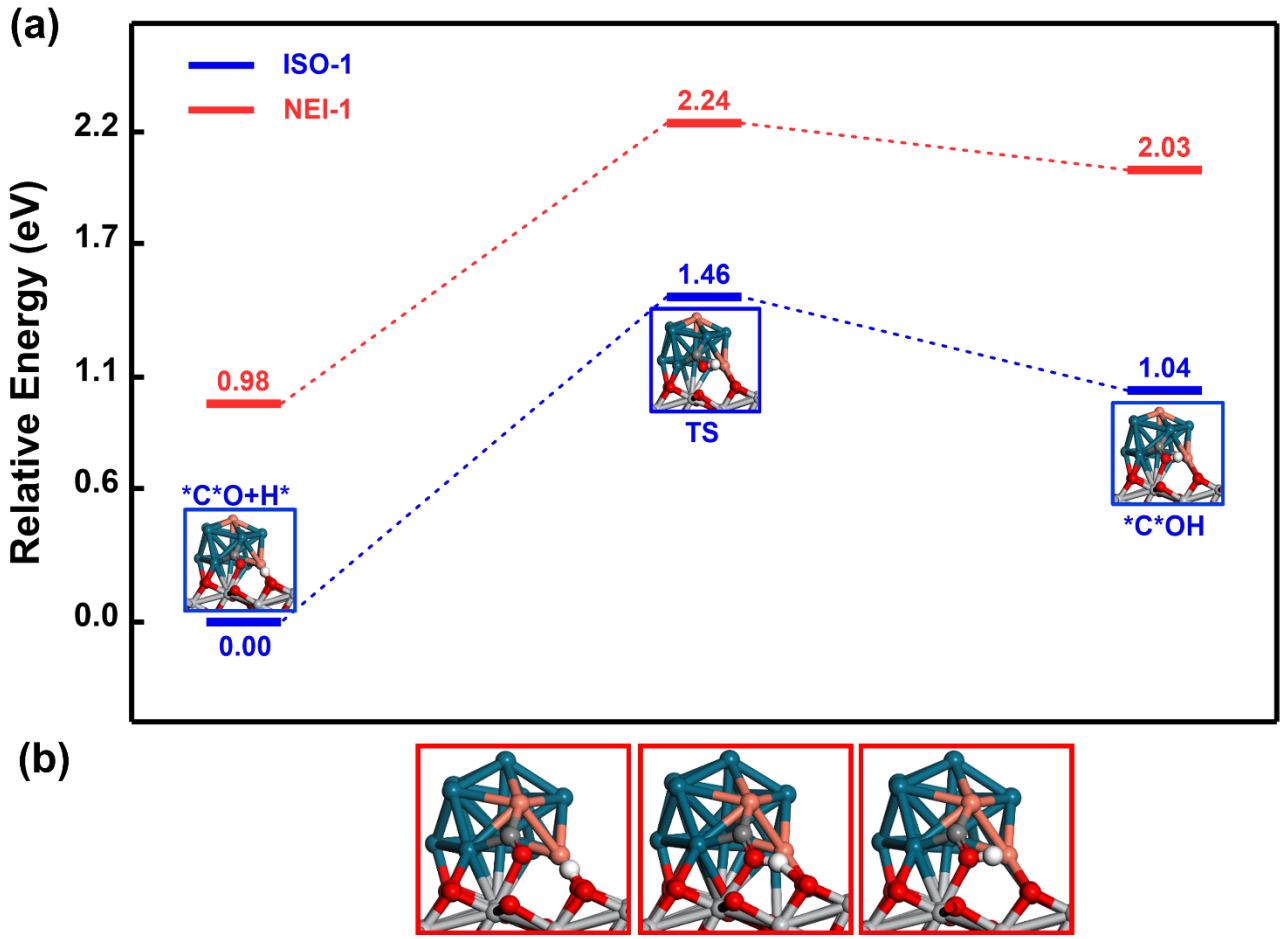

Figure S9. (a) The reaction pathways for *C*O to *C*OH related to the ISO-1 and NEI-1 models of $Pd_{11}Cu_2@TiO_2$, in which *O is first hydrogenated. Also shown are transition state and intermediate configurations related to ISO-1 and NEI-1 in panels a (ISO-1) and b (NEI-1). ISO-2 and NEI-2 cannot stabilize the *C*OH intermediate. Ti, O, Pd, Cu, C, and H atoms are in gray, red, cyan, orange, dark grey, and white, respectively.

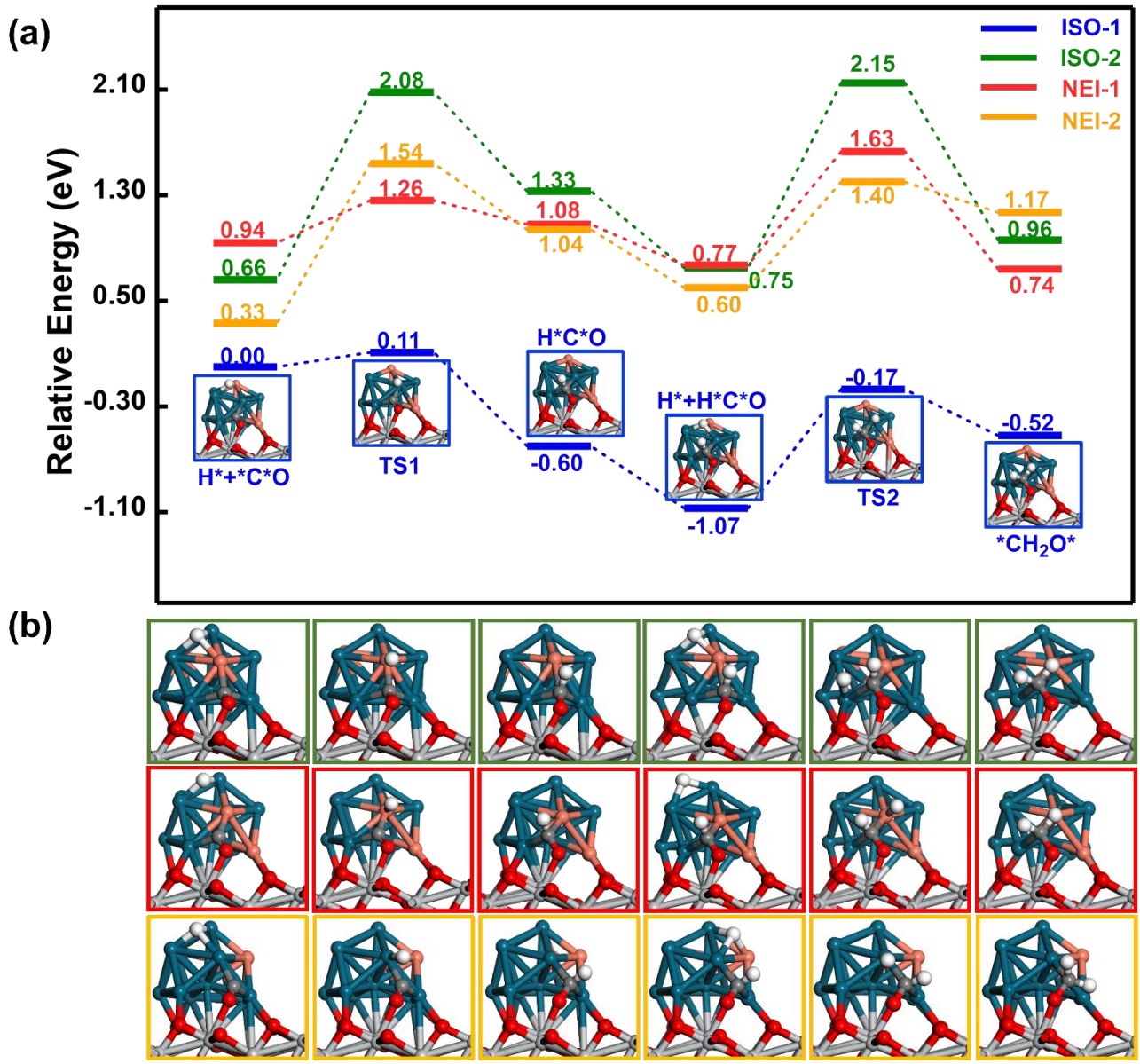

Figure S10. (a) The reaction pathways for *C*O to *CH_2O* related to the four interface models (ISO-1, ISO-2, NEI-1, and NEI-2) of $Pd_{11}Cu_2$@TiO_2, in which *C is consecutively hydrogenated. Relevant transition states and intermediates related to these four models are also shown in panels a (ISO-1) and b (ISO-2, NEI-1, and NEI-2). Ti, O, Pd, Cu, C, and H atoms are in gray, red, cyan, orange, dark grey, and white, respectively.

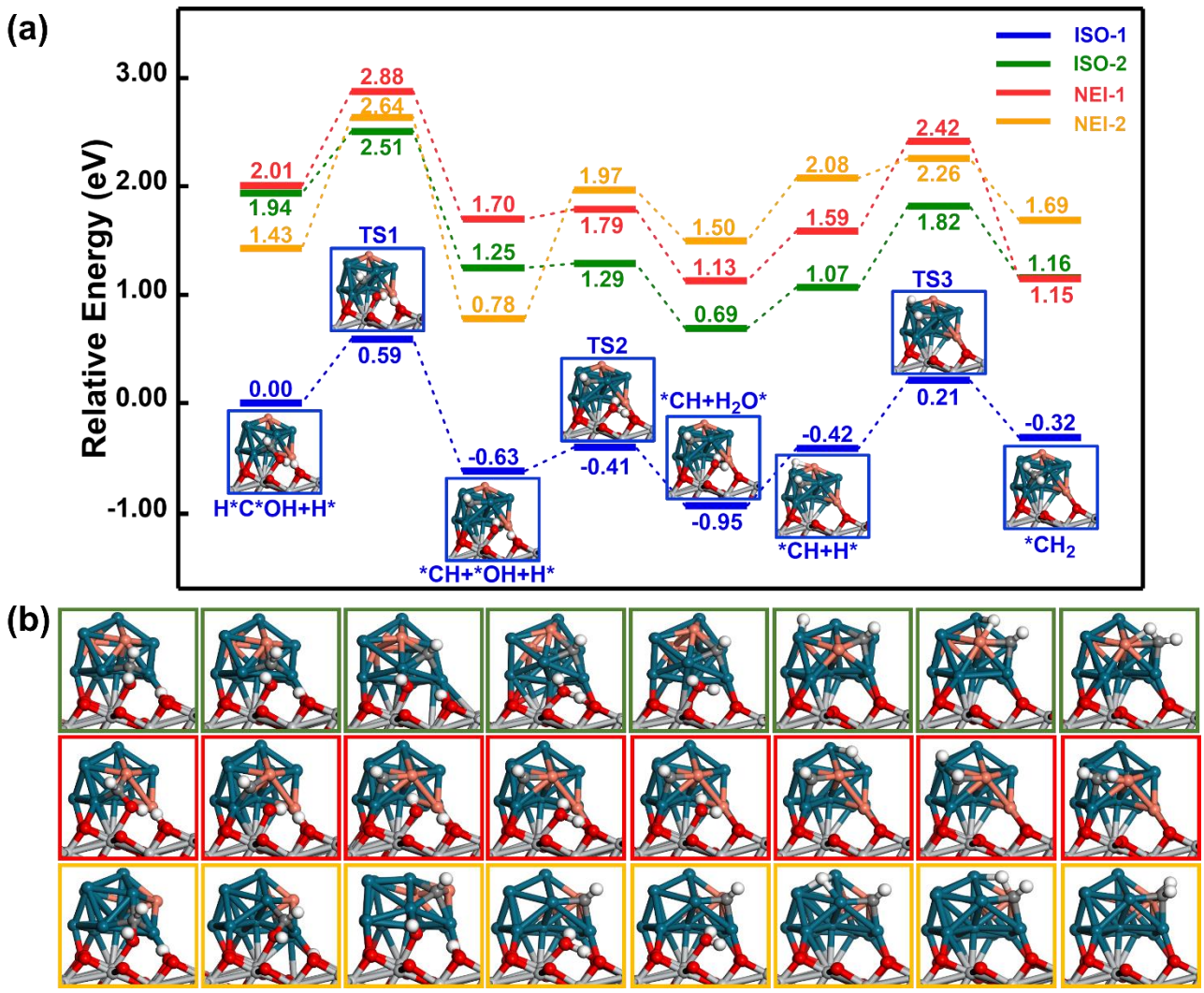

Figure S11. (a) The reaction pathways for H*C*OH to *CH_2 related to the four interface models (ISO-1, ISO-2, NEI-1, and NEI-2) of $Pd_{11}Cu_2$@TiO_2, in which H*C*OH dissociates its C-O bond, and *CH and *OH are hydrogenated to *CH_2 and H_2O*. Relevant transition states and intermediates related to these four models are also shown in panels a (ISO-1) and b (ISO-2, NEI-1, and NEI-2). Ti, O, Pd, Cu, C, and H atoms are in gray, red, cyan, orange, dark grey, and white, respectively.

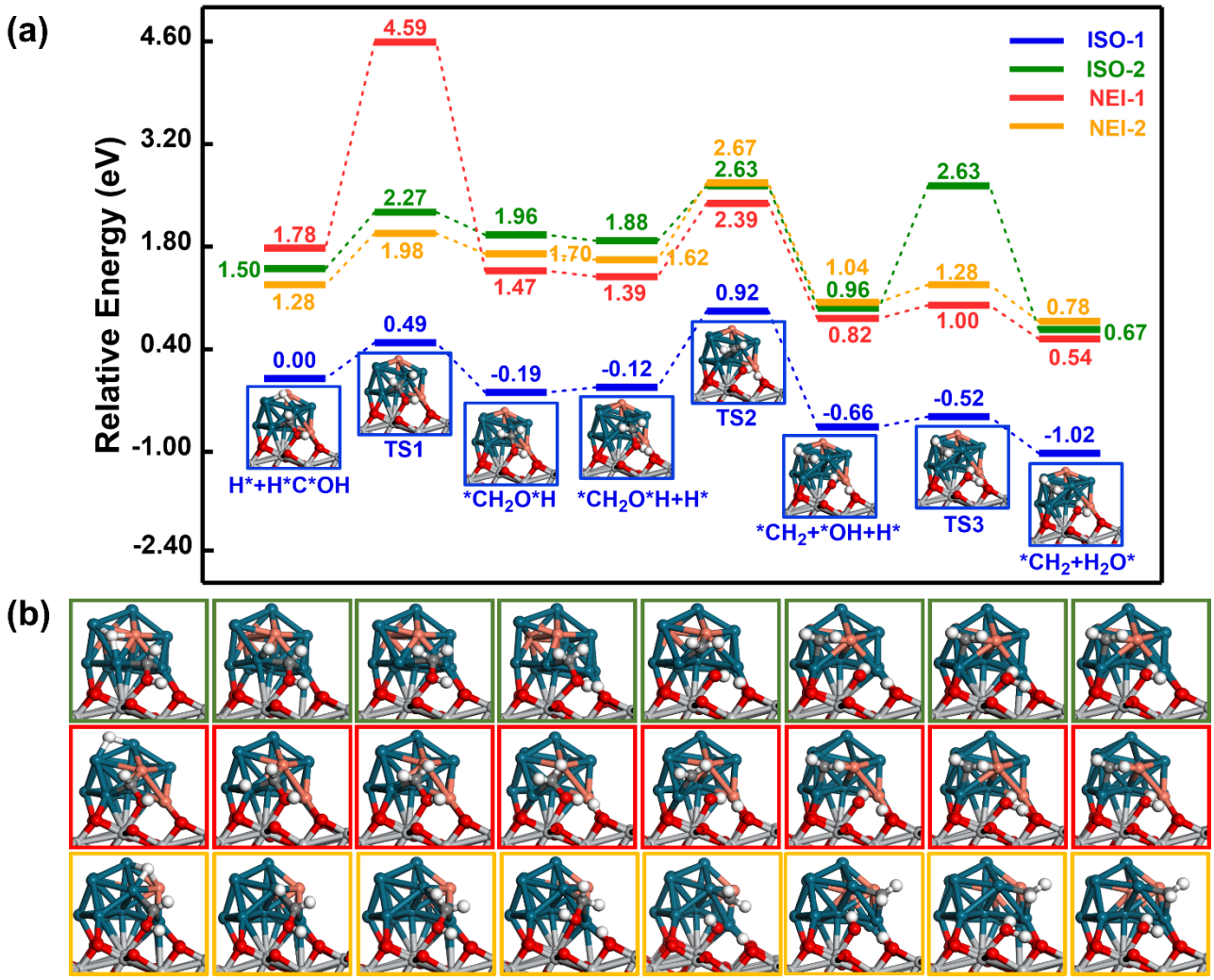

Figure S12. (a) The reaction pathways for H*C*OH to *CH_2 related to the four interface models (ISO-1, ISO-2, NEI-1, and NEI-2) of $Pd_{11}Cu_2$@TiO_2, in which H*C*OH is hydrogenated to produce *CH_2O*H, followed by the cleavage of the C-O bond. Relevant transition states and intermediates related to these four models are also shown in panels a (ISO-1) and b (ISO-2, NEI-1, and NEI-2). Ti, O, Pd, Cu, C, and H atoms are in gray, red, cyan, orange, dark grey, and white, respectively.

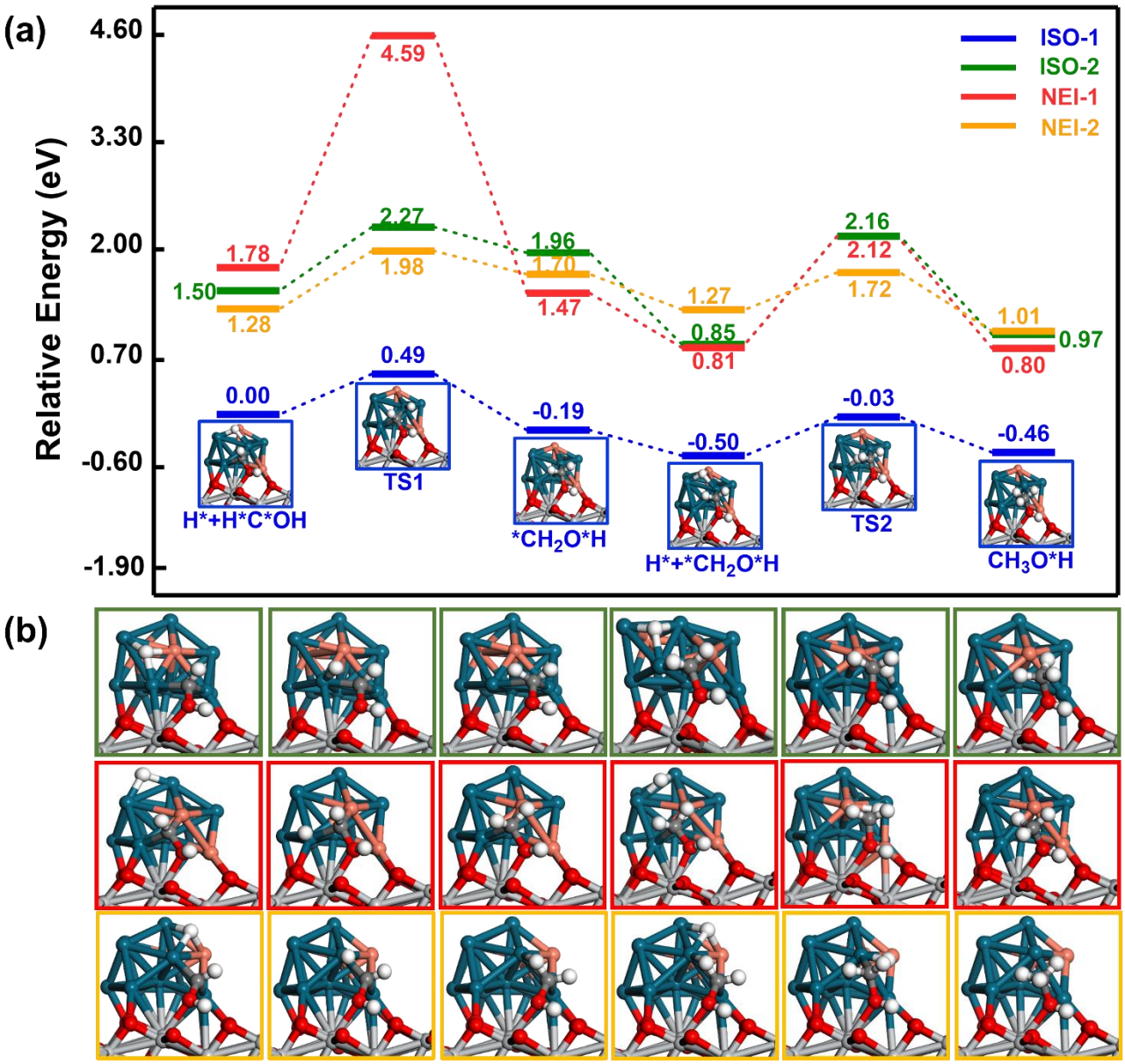

Figure S13. (a) The reaction pathways for H*C*OH to CH_3O*H related to the four interface models (ISO-1, ISO-2, NEI-1, and NEI-2) of $Pd_{11}Cu_2$@TiO_2. Relevant transition states and intermediates related to these four models are also shown in panels a (ISO-1) and b (ISO-2, NEI-1, and NEI-2). Ti, O, Pd, Cu, C, and H atoms are in gray, red, cyan, orange, dark grey, and white, respectively.

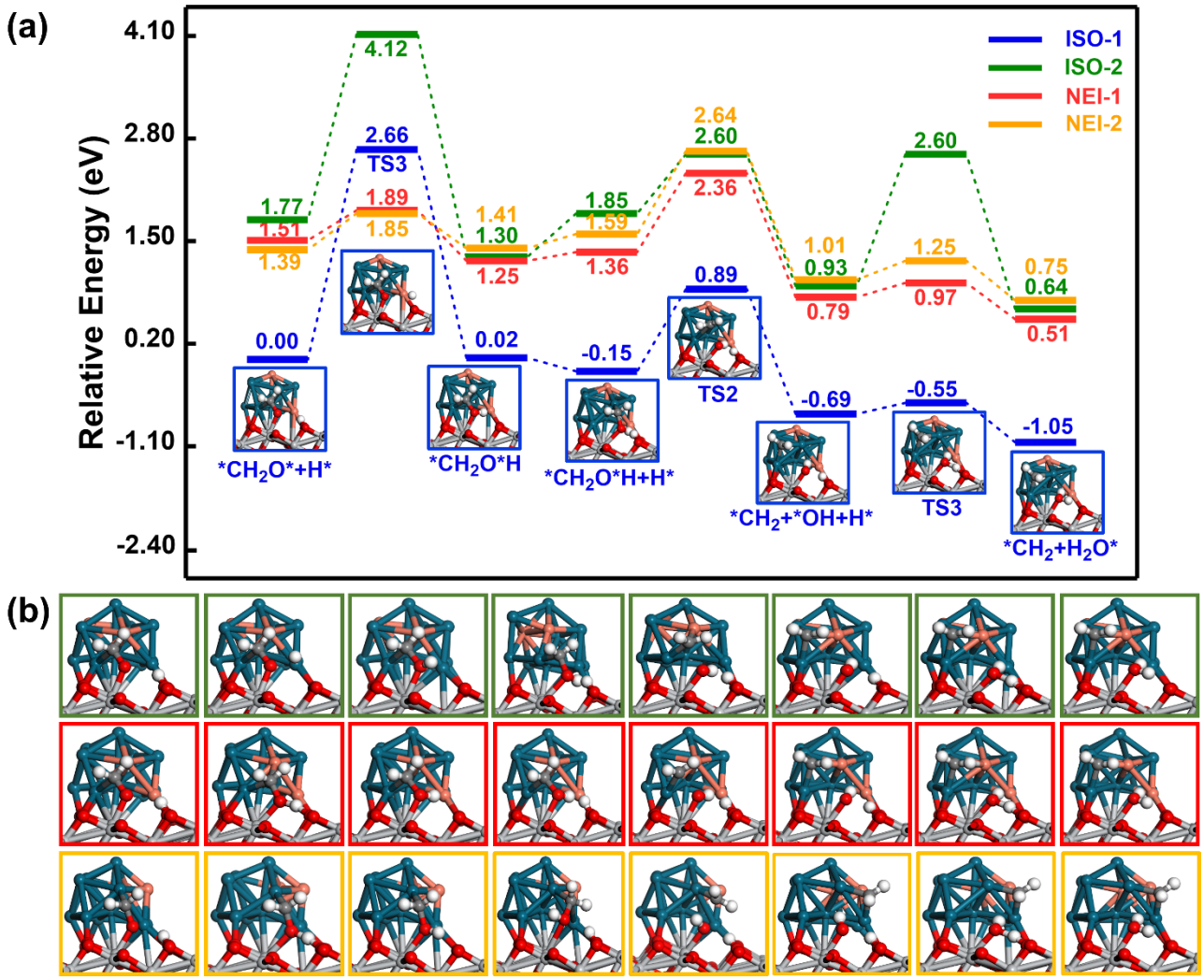

Figure S14. (a) The reaction pathways for *CH_2O* to *CH_2 related to the four interface models (ISO-1, ISO-2, NEI-1, and NEI-2) of $Pd_{11}Cu_2$@TiO_2, in which *CH_2O* is hydrogenated to produce *CH_2O*H, followed by the cleavage of the C-O bond. Relevant transition states and intermediates related to these four models are also shown in panels a (ISO-1) and b (ISO-2, NEI-1, and NEI-2). Ti, O, Pd, Cu, C, and H atoms are in gray, red, cyan, orange, dark grey, and white, respectively.

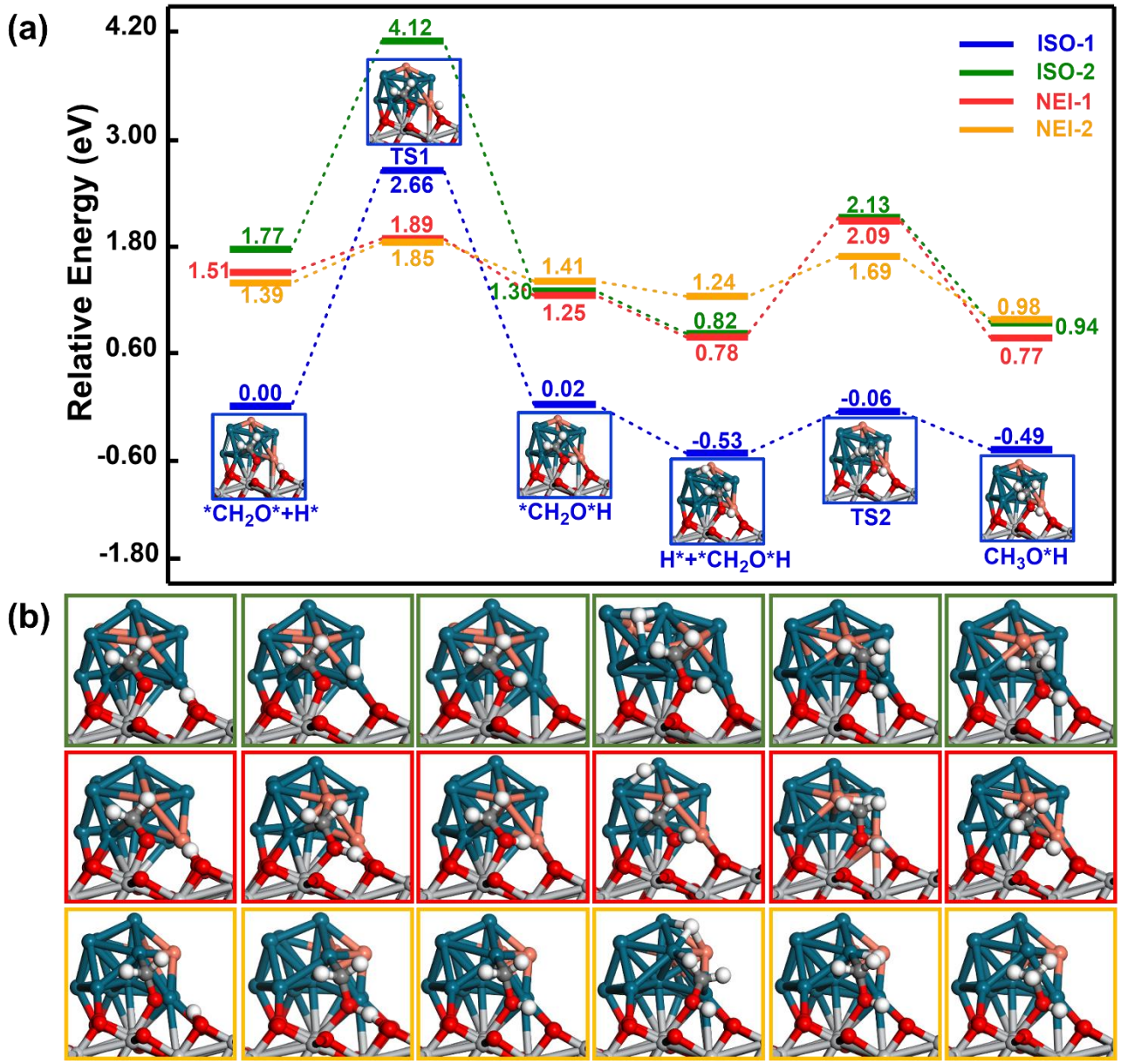

Figure S15. (a) The reaction pathways for *CH_2O* to CH_3O*H related to the four interface models (ISO-1, ISO-2, NEI-1, and NEI-2) of $Pd_{11}Cu_2$@TiO_2, in which *CH_2O* is sequentially hydrogenated to produce *CH_2O*H and CH_3O*H. Relevant transition states and intermediates related to these four models are also shown in panels a (ISO-1) and b (ISO-2, NEI-1, and NEI-2). Ti, O, Pd, Cu, C, and H atoms are in gray, red, cyan, orange, dark grey, and white, respectively.

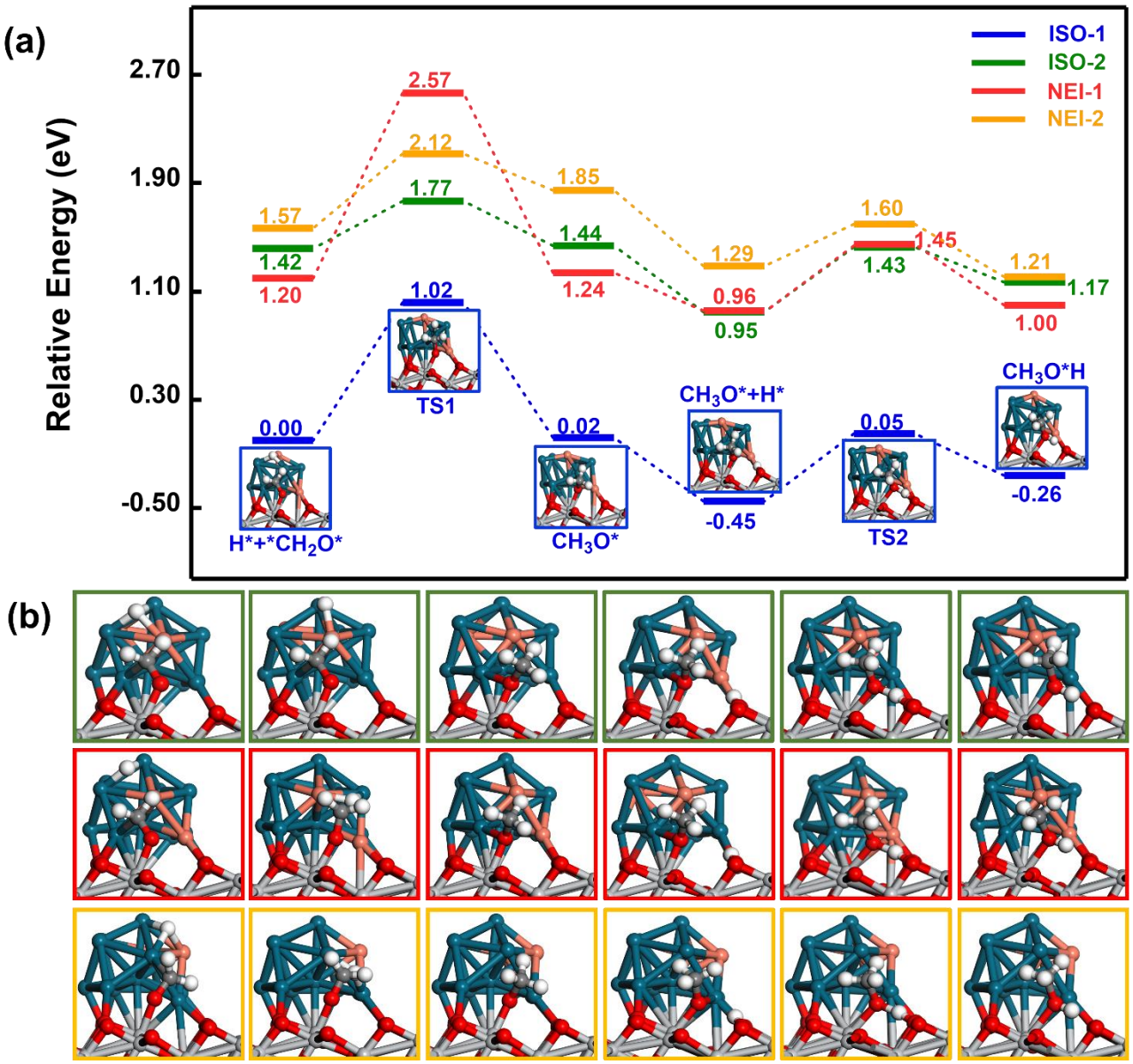

Figure S16. (a) The reaction pathways for *CH_2O* to CH_3O*H related to the four interface models (ISO-1, ISO-2, NEI-1, and NEI-2) of $Pd_{11}Cu_2$@TiO_2, in which *CH_2O* is sequentially hydrogenated to produce *CH_3O* and CH_3O*H. Relevant transition states and intermediates related to these four models are also shown in panels a (ISO-1) and b (ISO-2, NEI-1, and NEI-2). Ti, O, Pd, Cu, C, and H atoms are in gray, red, cyan, orange, dark grey, and white, respectively.

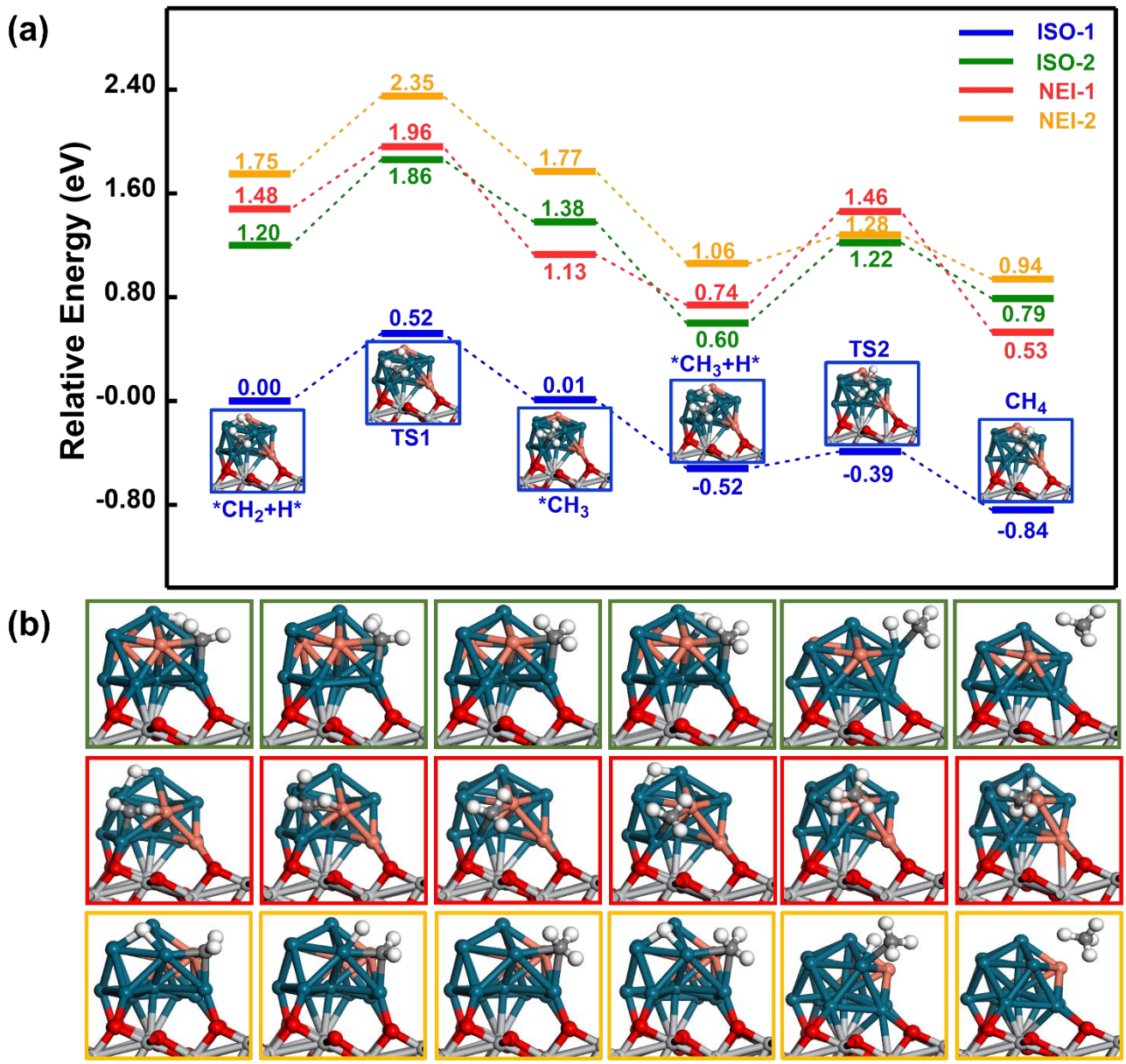

Figure S17. (a) The reaction pathways for *CH_2 to CH_4 related to the four interface models (ISO-1, ISO-2, NEI-1, and NEI-2) of $Pd_{11}Cu_2$@TiO_2. Relevant transition states and intermediates related to these four models are also shown in panels a (ISO-1) and b (ISO-2, NEI-1, and NEI-2). Ti, O, Pd, Cu, C, and H atoms are in gray, red, cyan, orange, dark grey, and white, respectively.

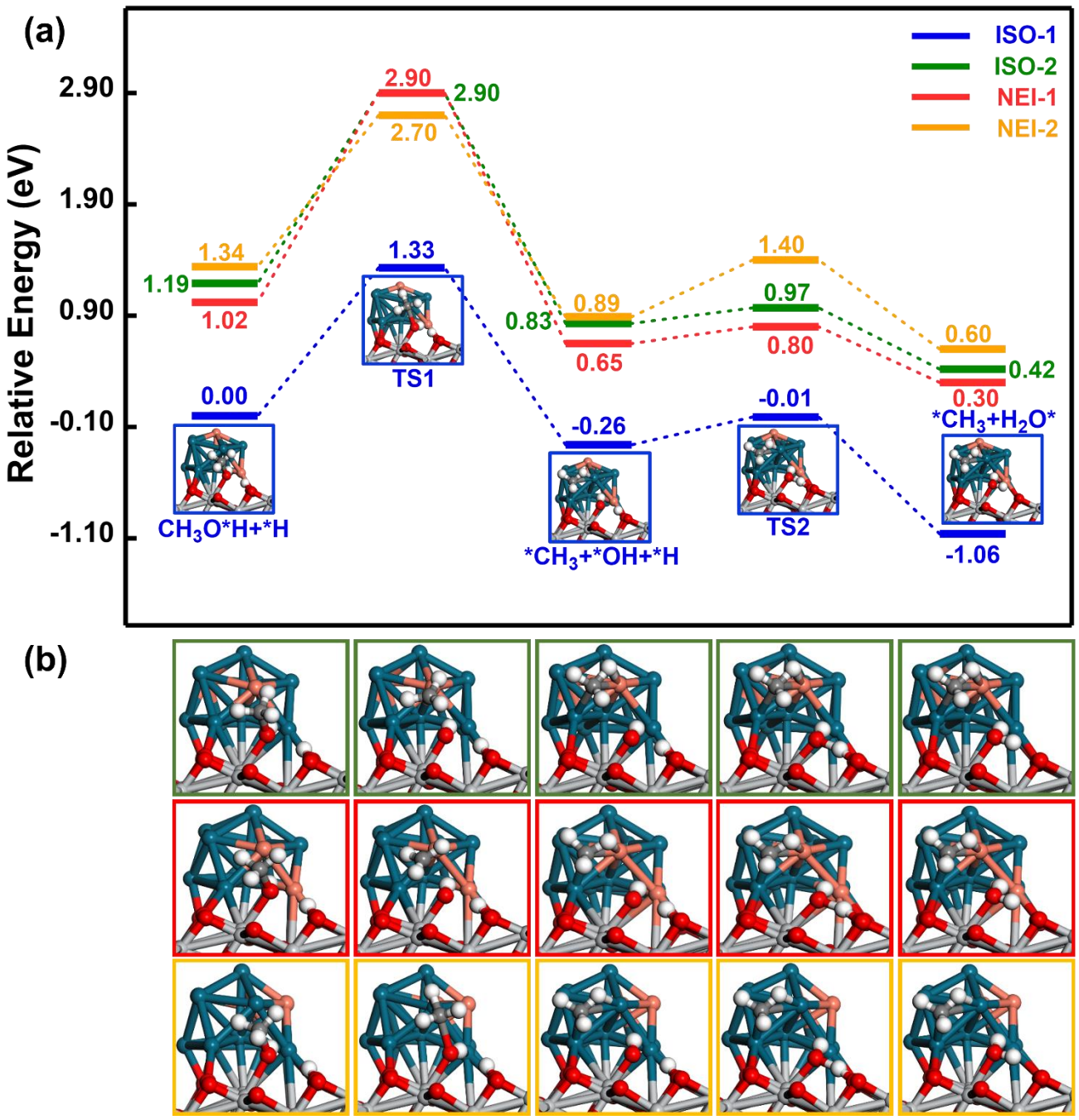

Figure S18. (a) The reaction pathways for CH_3O*H to *CH_3 related to the four interface models (ISO-1, ISO-2, NEI-1, and NEI-2) of $Pd_{11}Cu_2$@TiO_2. Relevant transition states and intermediates related to these four models are also shown in panels a (ISO-1) and b (ISO-2, NEI-1, and NEI-2). Ti, O, Pd, Cu, C, and H atoms are in gray, red, cyan, orange, dark grey, and white, respectively.

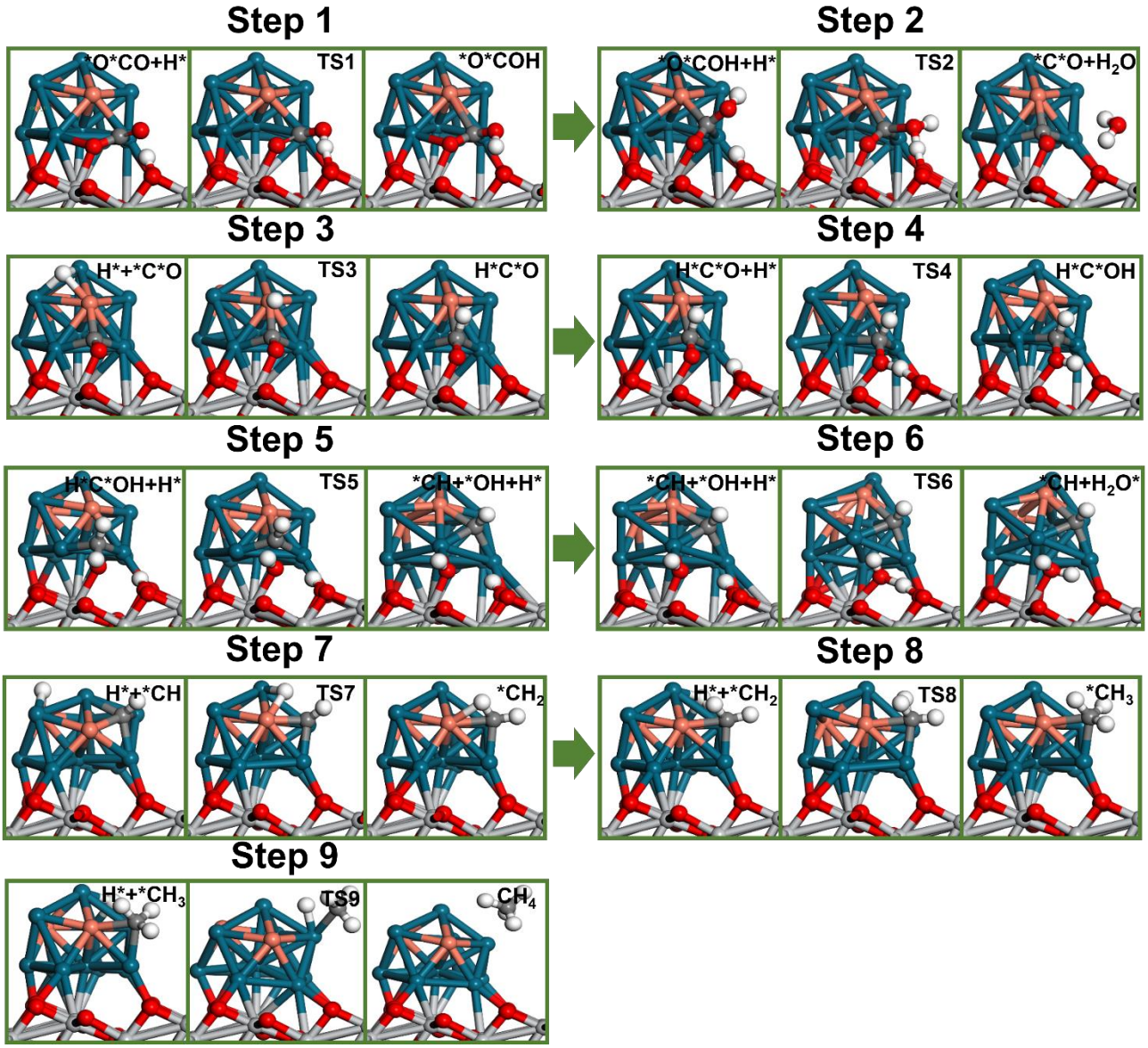

Figure S19. The transition states and intermediates along the most efficient pathway for the CH_4 formation related to the ISO-2 model of $Pd_{11}Cu_2@TiO_2$.

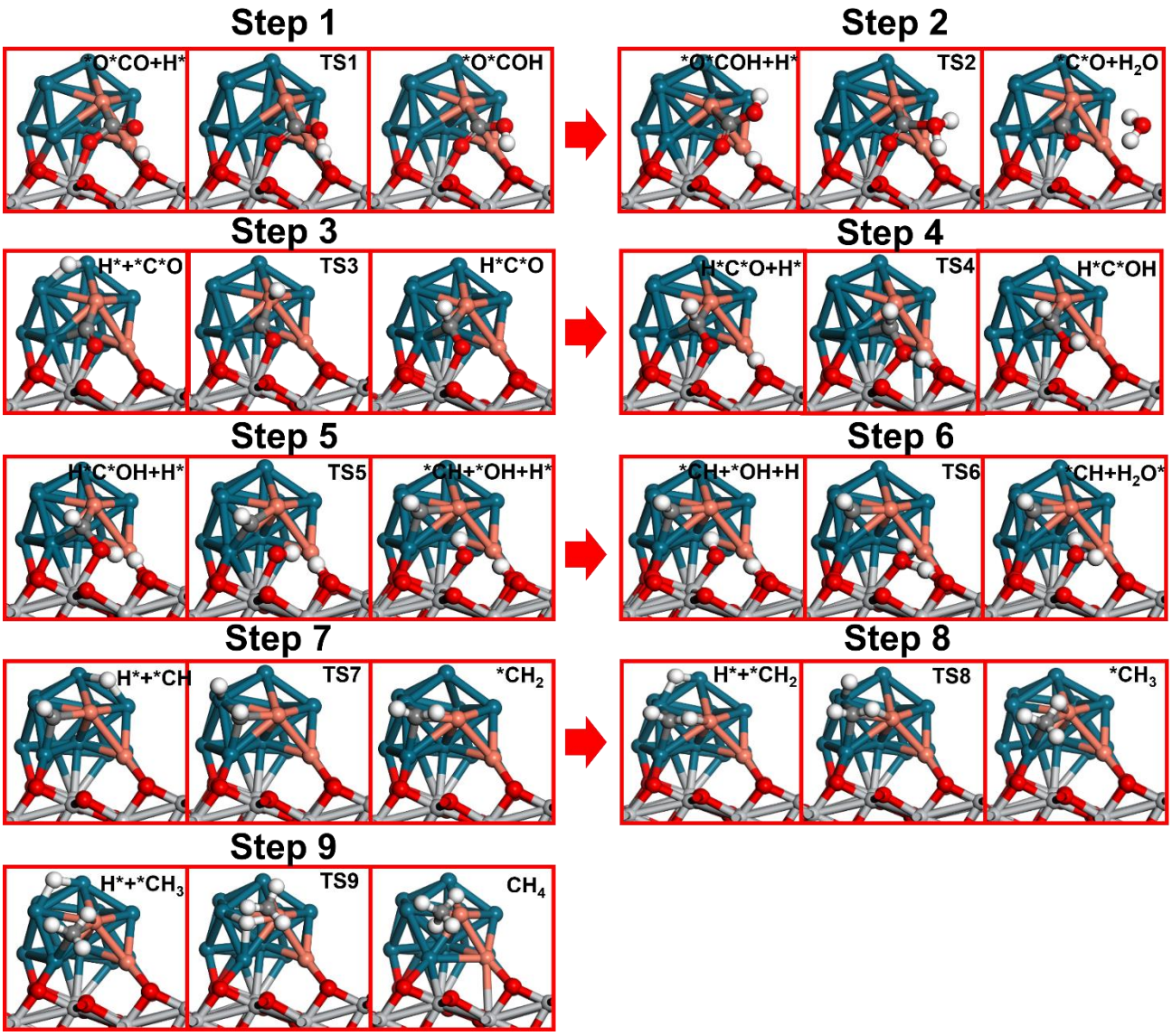

Figure S20. The transition states and intermediates along the most efficient pathway for the CH_4 formation related to the NEI-1 model of $Pd_{11}Cu_2@TiO_2$.

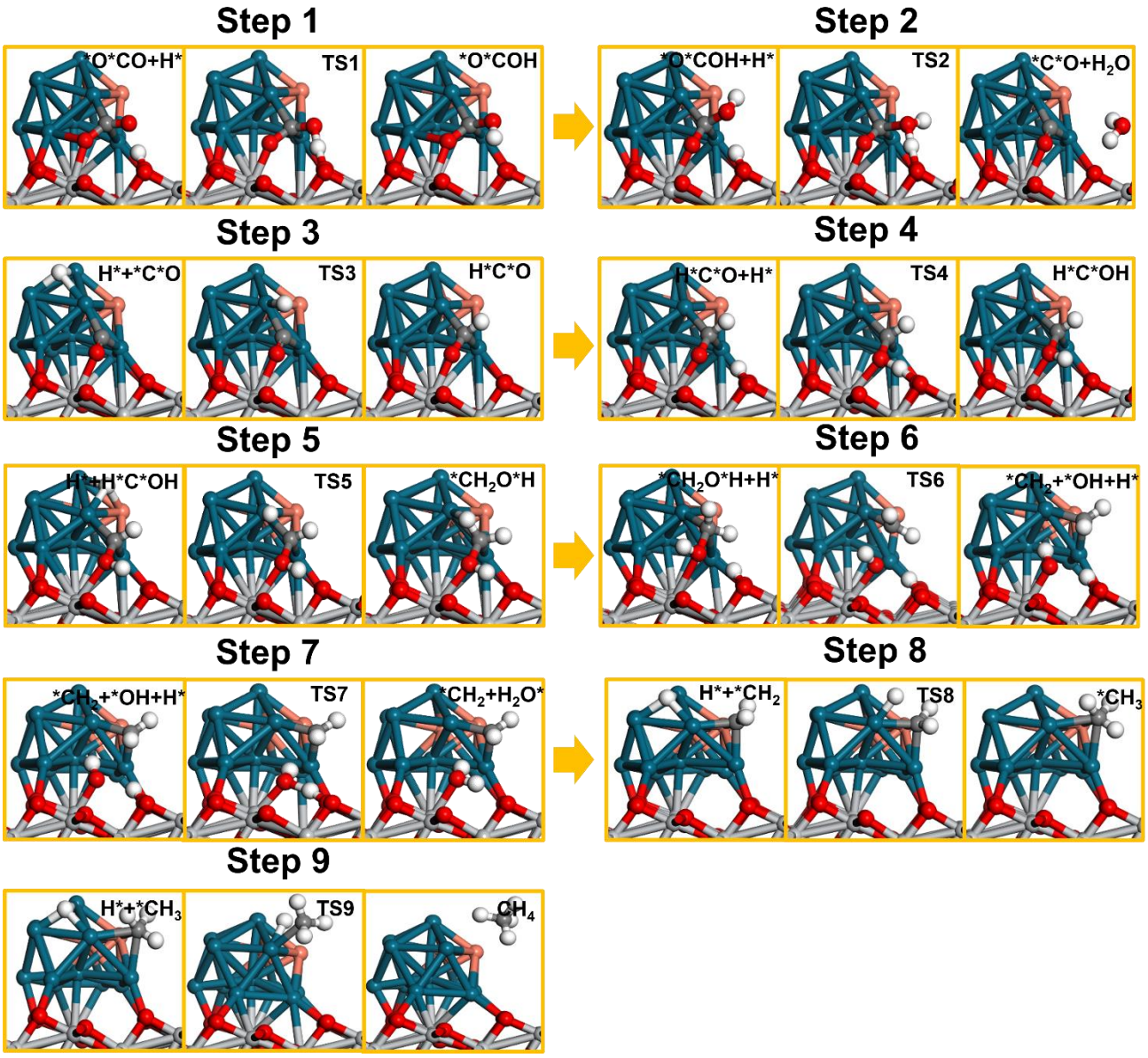

Figure S21. The transition states and intermediates along the most efficient pathway for the CH_4 formation related to the NEI-2 model of $Pd_{11}Cu_2@TiO_2$.

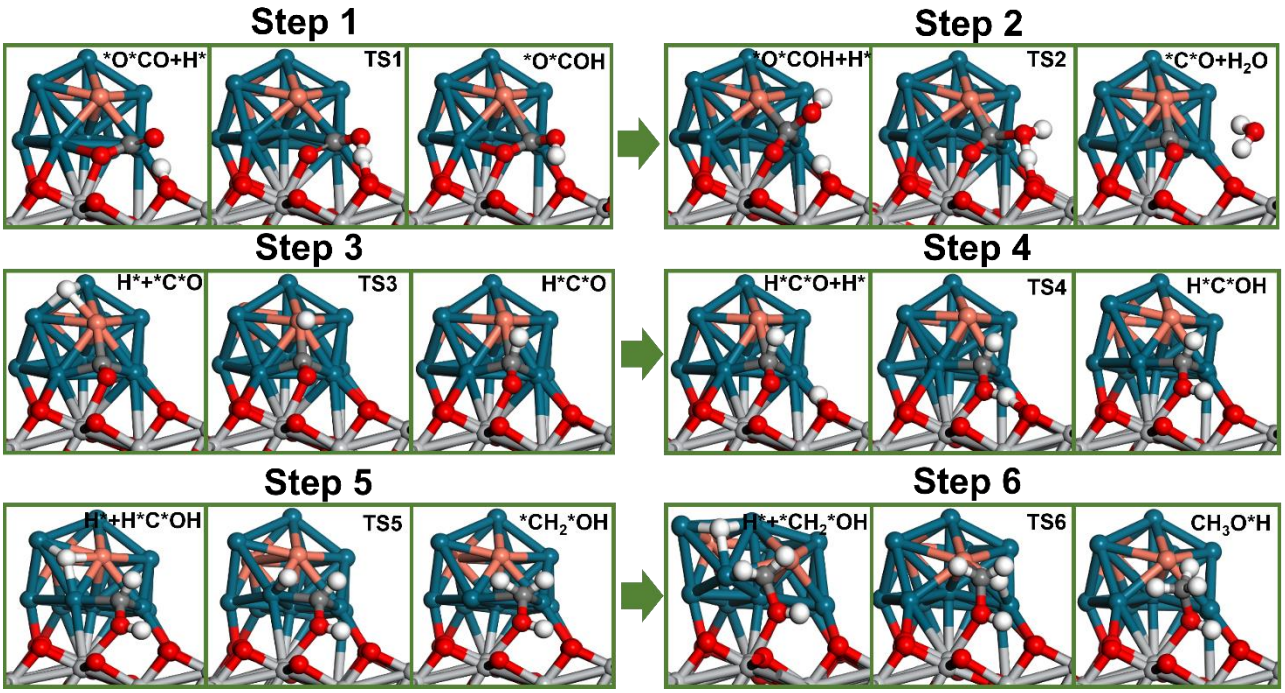

Figure S22. The transition states and intermediates along the most efficient pathway for the CH_3OH formation related to the ISO-2 model of $Pd_{11}Cu_2@TiO_2$.

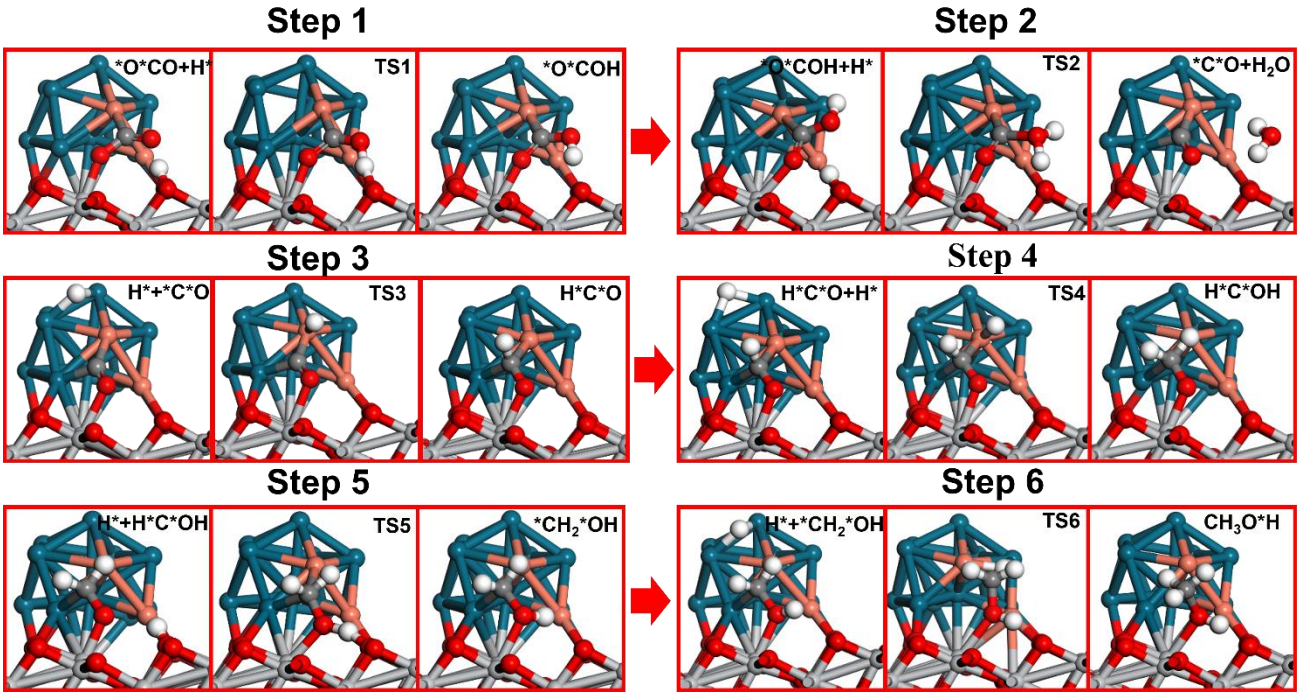

Figure S23. The transition states and intermediates along the most efficient pathway for the CH_3OH formation related to the NEI-1 model of $Pd_{11}Cu_2@TiO_2$.

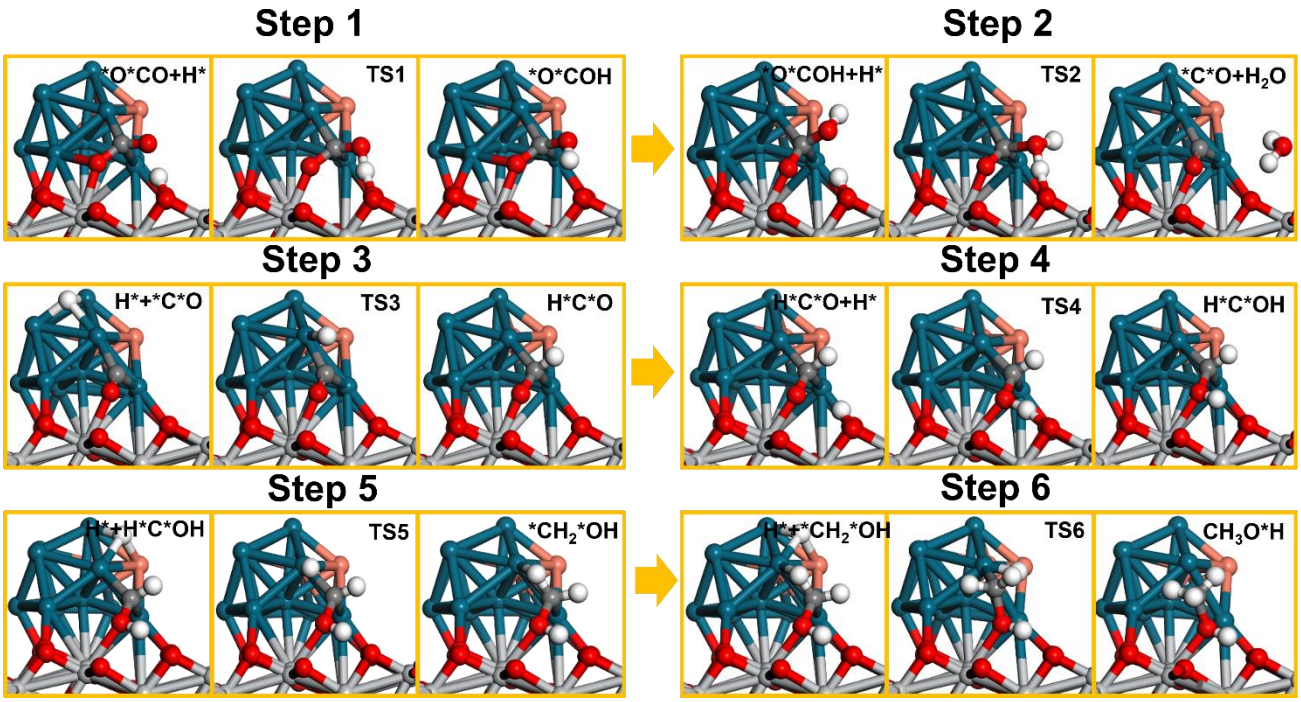

Figure S24. The transition states and intermediates along the most efficient pathway for the CH_3OH formation related to the NEI-2 model of $Pd_{11}Cu_2@TiO_2$.

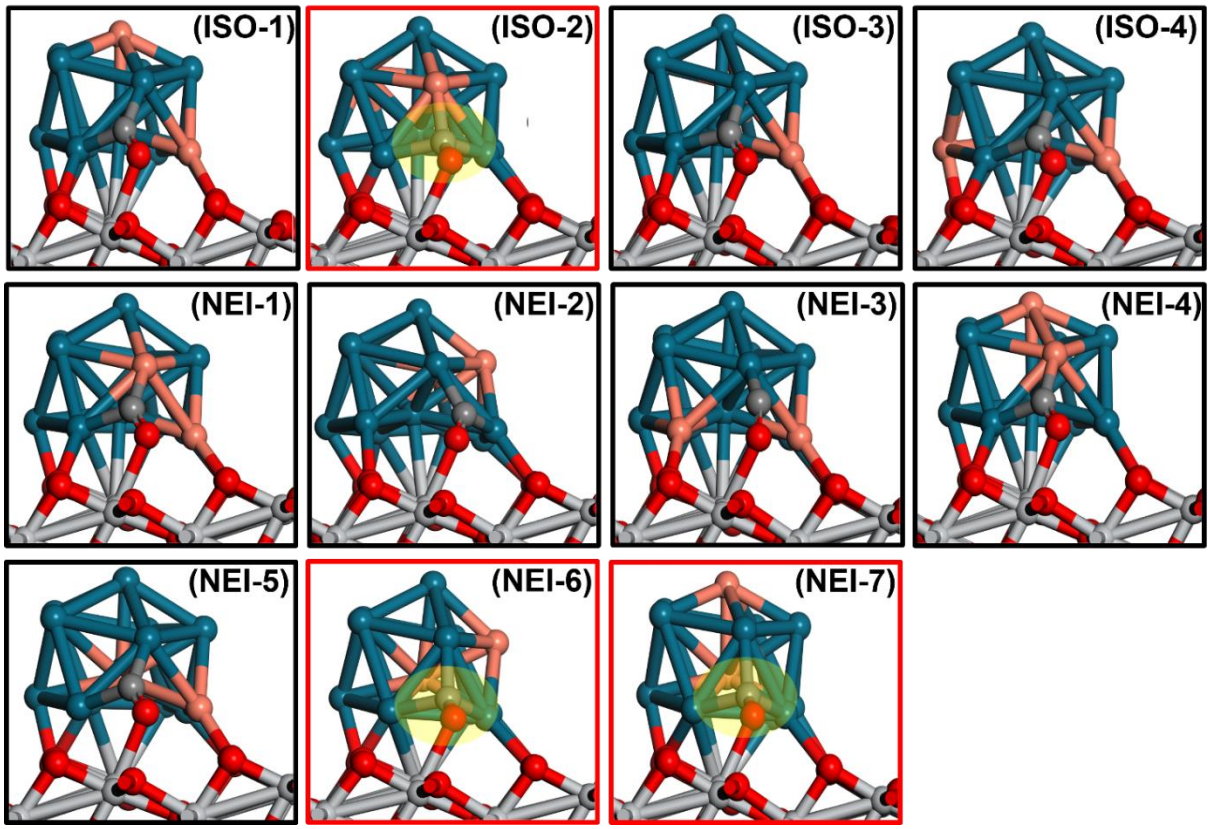

Figure S25. The *C*O adsorbed configurations related to the eleven models of $Pd_{11}Cu_2@TiO_2$ (ISO-1 to ISO-3, and NEI-1 to NEI-7). The *C*O structures in a valence-bond saturated state are highlighted.

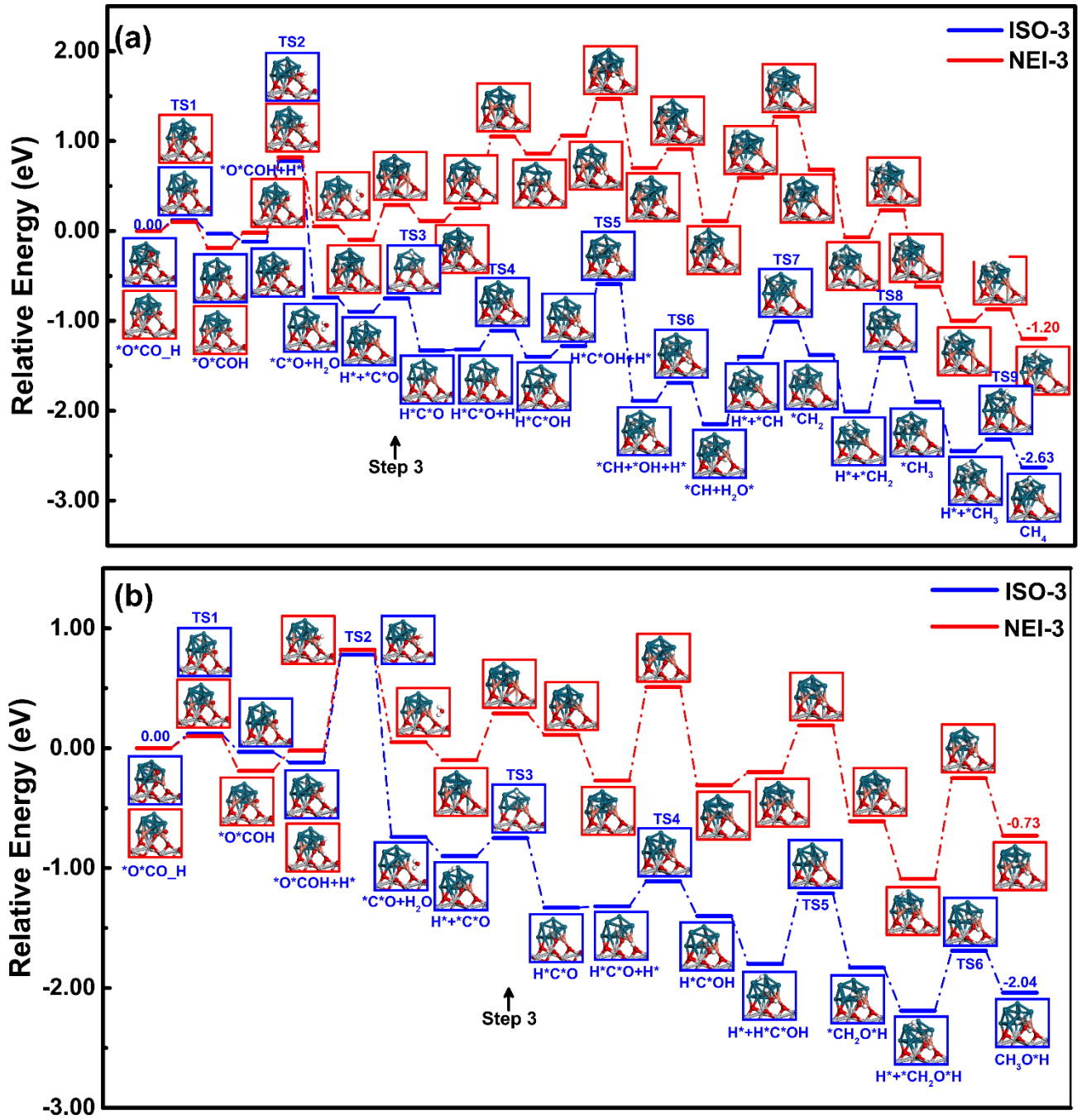

Figure S26. The most efficient reaction pathways for CO_2 reduction to (a) CH_4 and (b) CH_3OH related to the ISO-3 and NEI-3 models of $Pd_{11}Cu_2@TiO_2$. Also shown are transition states and intermediates.

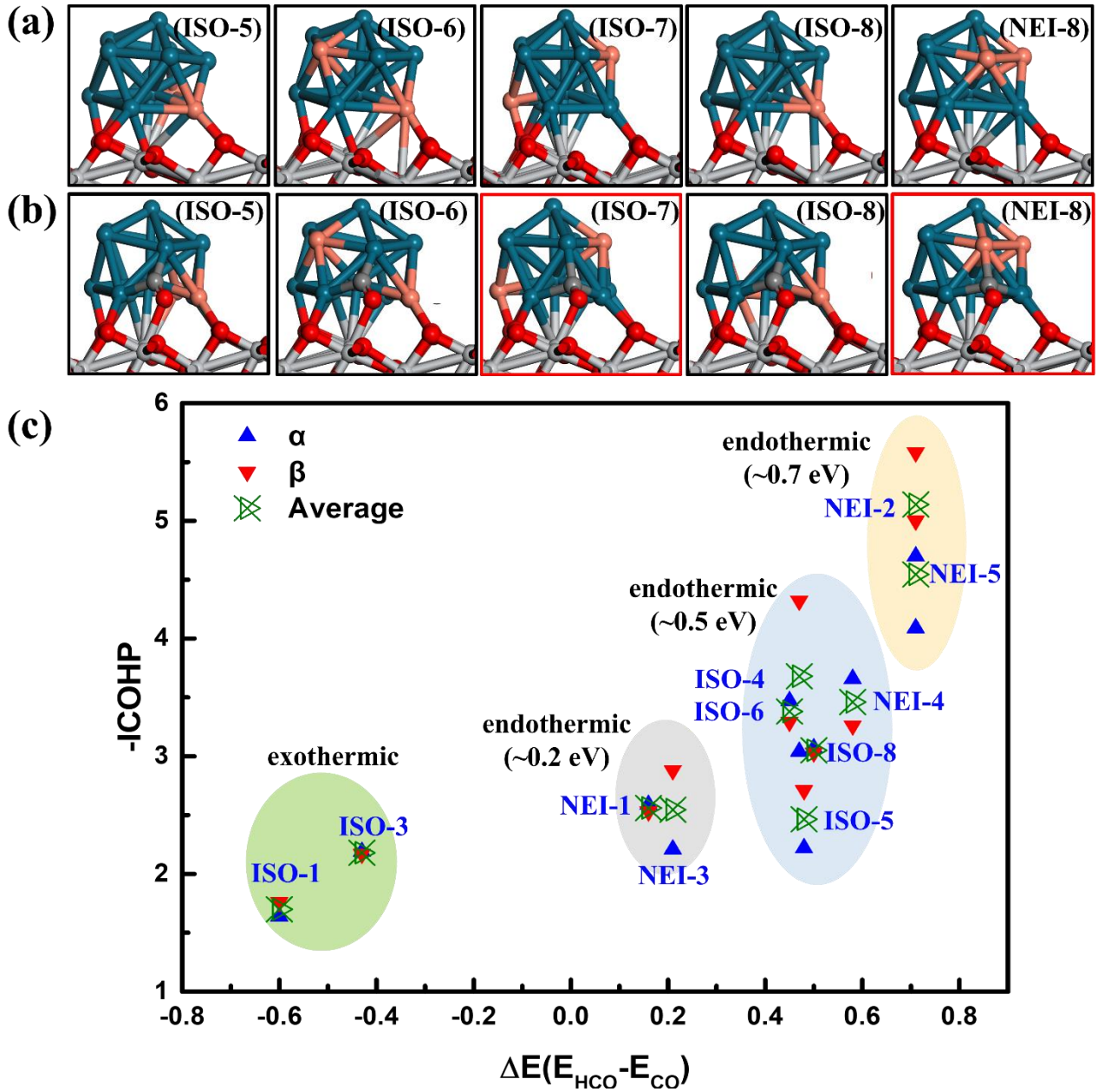

Figure S27. Five additional computational models developed for verification the reliability of the conclusions.

Section I: Microkinetic Simulation Details

The net rate for elementary step *i* in term of the forward rate constant, k_i, the coverage of reactant on two different sites, $\theta(\mathrm{j})$, and the reversibility, Z_i, can be written as[1]

$$r_i = k_i \prod_j \theta(\mathrm{j})^{\nu_{ij}} \left(1 - Z_i\right) \qquad [1]$$

where $Z_i = \frac{Q_i}{K_{i,eq}}$, which approaches 0 as step *i* becomes irreversible and approaches 1 as step *i* becomes quasi-equilibrated. $K_{i,eq}$ is the equilibrium constant of step *i*, determined by the standard Gibbs free energy change ($-\Delta G_i$) of the elementary reaction, $K_{eq,i} = \exp(-\frac{\Delta G_i}{RT})$. $Q_i = \frac{C_{1-}C_{2-}^{\cdots}\theta_{1-}\theta_{2-}^{\cdots}}{C_{1+}C_{2+}^{\cdots}\theta_{1+}\theta_{2+}^{\cdots}}$ is the reaction quotient of step *i*. The rate constant, k_i, for the elementary step can be determined by the transition state theory:

$$k_i = \frac{k_B T}{h}\exp(-\frac{\Delta G_i}{RT}) = \frac{k_B T}{h}\exp(\frac{\Delta S}{R})\exp(-\frac{E_a}{RT}) \approx \frac{k_B T}{h}\exp(-\frac{E_a}{RT}) \qquad [2]$$

where k_B and h are the Boltzmann and Planck constants, respectively. The standard equilibrium constant $K_{eq,i}$ and rate constant k_i can be calculated with DFT data including entropy and zero-point energy effects. Under the steady-state approximation, we can solve a set of kinetic equations with the condition that the coverages on each adsorption site are equal to 1.

To evaluate the relative significance of each elementary step in influencing the overall catalytic activity, the "degree of rate control" ($X_{RC,i}$) is utilized[2-3]. This technique provides a quantitative assessment of the sensitivity of each step within the comprehensive reaction framework. $X_{RC,i}$ for step *i* can be expressed in term of the standard Gibbs free energy of the transition state as

$$X_{RC,i} = \frac{k_i}{r}\left(\frac{\partial r}{\partial k_i}\right)_{j\neq i,Keq,i} = \left(\frac{\partial \ln r}{\partial \ln k_i}\right)_{j\neq i,K_{eq,i}} \qquad [3]$$

The value of $X_{RC,i}$ for step *i* is larger, the influence of this step on the overall reaction rate is bigger.

Here we used the collision theory to handle the kinetics of molecular adsorption process and to derive the equivalent barriers (E_a). According to the transition state and collision theories, the reaction rate on a per-site basis can be written as:

$$r_+(T) = \frac{k_B T}{h} \exp(-\frac{E_a}{k_B T}) \frac{P_i}{P^0} \approx S_i(T) \frac{P_i A_0}{\sqrt{2\pi k_B m_i T}} \quad [4]$$

where k_B , h , T , P_i and m_i are the Boltzmann constant, Planck constant, reaction temperature, pressure, and mass of gas molecule, respectively. A_0 is the area of the atom which is described as $A_0 = \pi^* r^2$, in which *r* is the VDW radius of the atom. Herein, we have assumed that the gas molecule behaves ideally, $S_i(T)$, the sticking coefficient, is seen as 1. Hence, we could get an equation about E_a :

$$E_a \approx -k_B T \ln(\frac{P^0 A_0 h}{k_B T \sqrt{2\pi k_B m_i T}}) \quad [5]$$

In the present microkinetic simulation, we followed the experimental condition[4], 2 atm CO_2, $6*10^{-5}$ atm CH_4, $5.7*10^{-6}$ atm CO, $4.5*10^{-6}$ atm H_2, and T = 300 K. Also, the concentration of liquid H_2O was set as 55.6 mol/L (pure water), and the concentration of liquid products HCOOH and CH_3OH were assumed to be 1 and 1 mol/L. C_h^+ and C_e- are set as 10^{-9} mol/L[5-6].

Section II: Water Photolysis

To account for the microkinetic simulation requirements of intermediates of H^+ and H, we also explored the photocatalytic H_2O splitting, including water oxidation to produce O_2 and water reduction to generate H_2, which is considered one of the major competitors to the CO_2 reduction.

In the first step, water dissociates to form OH^-/H^+, or OH^-/H (H^+ withdrawing an e^- from $Pd_{11}Cu_2$). The production of H^+ or H depends on the adsorption site of the dissociated H species. If it is adsorbed on O_{2b}, H^+ is formed (as shown by path I in Figure S28); if it is adsorbed on the $Pd_{11}Cu_2$ cluster, an H atom is formed (as indicated by path II in Figure S28). From a thermodynamic standpoint, the two product formation pathways are competitive, as both are endothermic by ca. 0.2 eV. However, the pathway for H^+ is more favorable due to its lower energy barrier (0.70 eV compared to 1.00 eV for H). According to our calculations, the first step of water dissociation involving holes is non-competitive, as it requires an endothermic energy input of 0.76 eV, similar to the previously reported dissociation of water on the TiO_2 surface[5-7].

The two adsorption configurations of OH^- produced in the first step undergo a subsequent H dissociation step. Similar to the initial step, depending on the adsorption structure of OH^-, the dissociated H may be adsorbed on O_{2b}, resulting in H^+, or onto the $Pd_{11}Cu_2$ cluster, leading to H. A key question remains whether holes are involved in this dissociation process. If OH^- dissociation occurs without the involvement of a hole, and the dissociated H atom is adsorbed on the $Pd_{11}Cu_2$ cluster, the reaction must overcome an energy barrier of 1.36 eV and absorb 0.47 eV energy to form the O^- intermediate (as shown by path I in Figure S29). Alternatively, if the dissociated H^+ is adsorbed on the O_{2b} site, the process requires an energy barrier of 0.99 eV and the energy absorption of 0.08 eV, resulting in the formation of the O^{2-} intermediate (path II in Figure S29). If a hole participates in the reaction, transferring the hole from the bulk to OH^- producing OH is endothermic, requiring ca. 0.2 eV (Figure S30) and an associated energy barrier of around 0.5 eV[8]. Based on this OH, when H^+ is adsorbed on the O_b site, forming O^-/H^+, the dissociation process needs to overcome an energy barrier of 0.33 eV and releases 0.10 eV energy. In contrast, for the formation of O/H with H adsorbed on the $Pd_{11}Cu_2$ cluster, the process requires overcoming a higher barrier of 0.89 eV and releases 0.17 eV energy (Figure S31). Comparatively, the involvement of a hole in the second step of the H_2O

dissociation is more favorable for facilitating the reaction. Subsequently, O^- can react with a hole to form O (Figure S32), and then two O atoms form O_2 (Figure S33). To identify the generated radicals, we analyze their geometric structures, spin densities, Bader charge and magnetic moments. The corresponding data are provided in Table S6 and Figure S29-33.

The H and H^+ produced from water dissociation can couple to form H_2. The formation of H_2 from H^+ is a major competing pathway in the CO_2 reduction. However, as shown in Figure S34, the H^+ reduction does not offer a competitive advantage over the CO_2 reduction, due to a high energy barrier of 2.24 eV for the H^+ reduction.

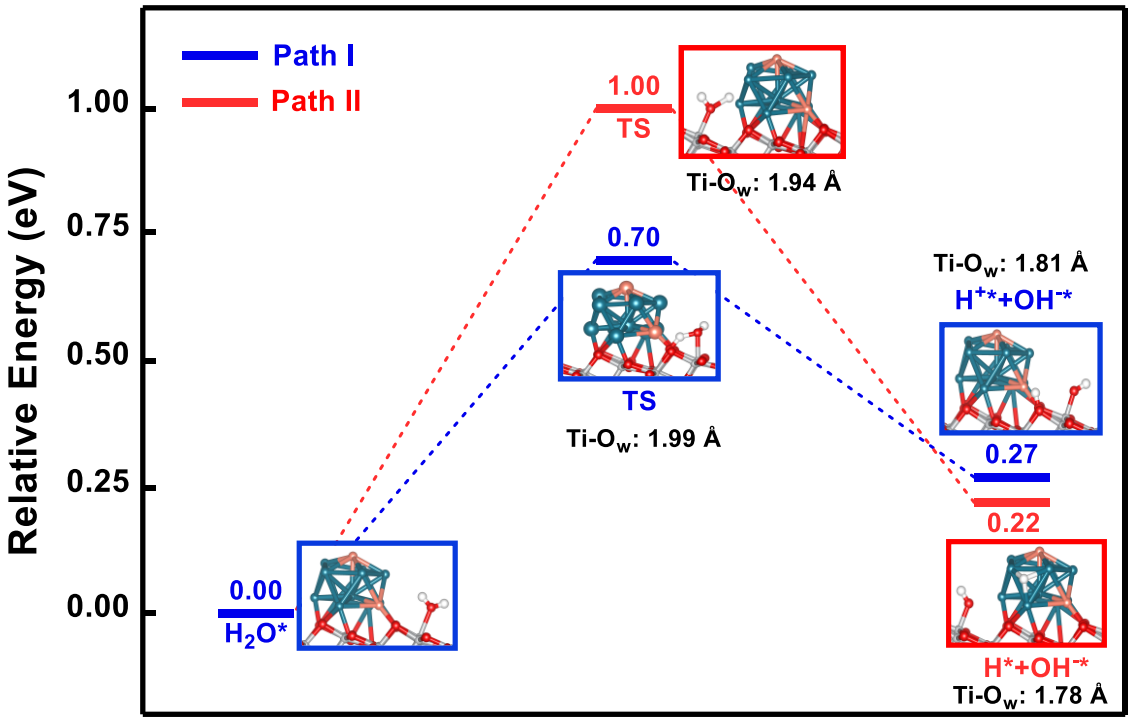

Figure S28. The reaction pathways for water dissociation yielding OH^-/H (path I) and OH^-/H^+ (path II) without hole involvement.

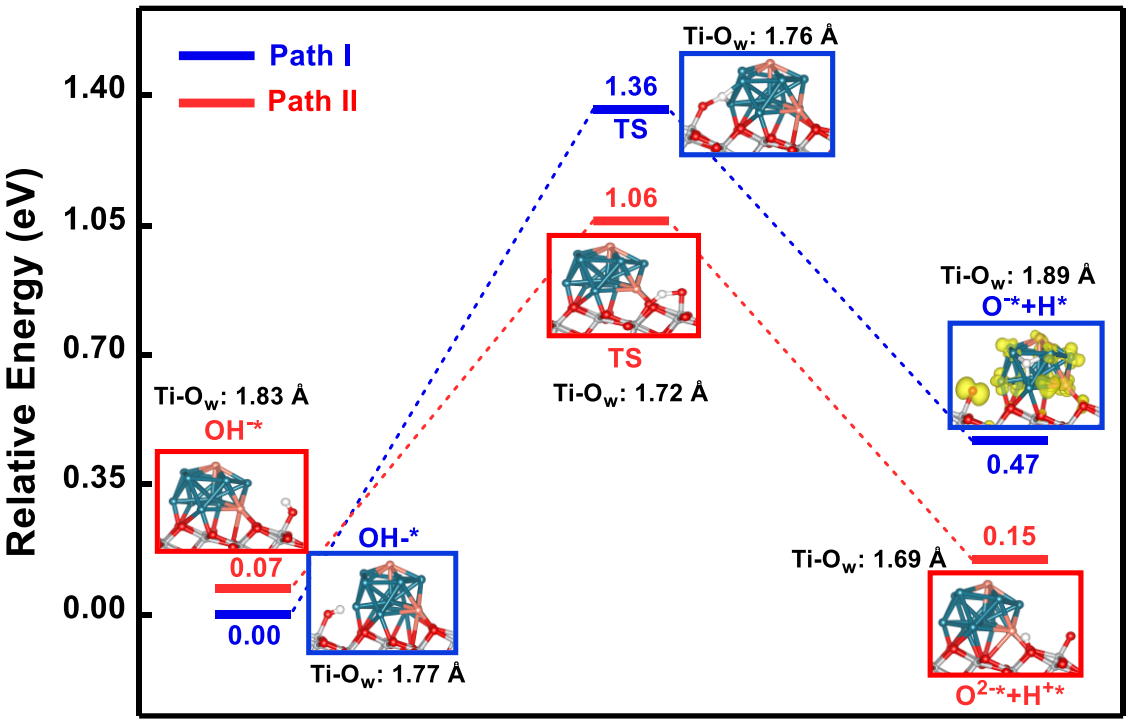

Figure S29. The reaction pathways for OH^- dissociation yielding O^-/H (path I) and O^{2-}/H^+ (path II) without hole involvement.

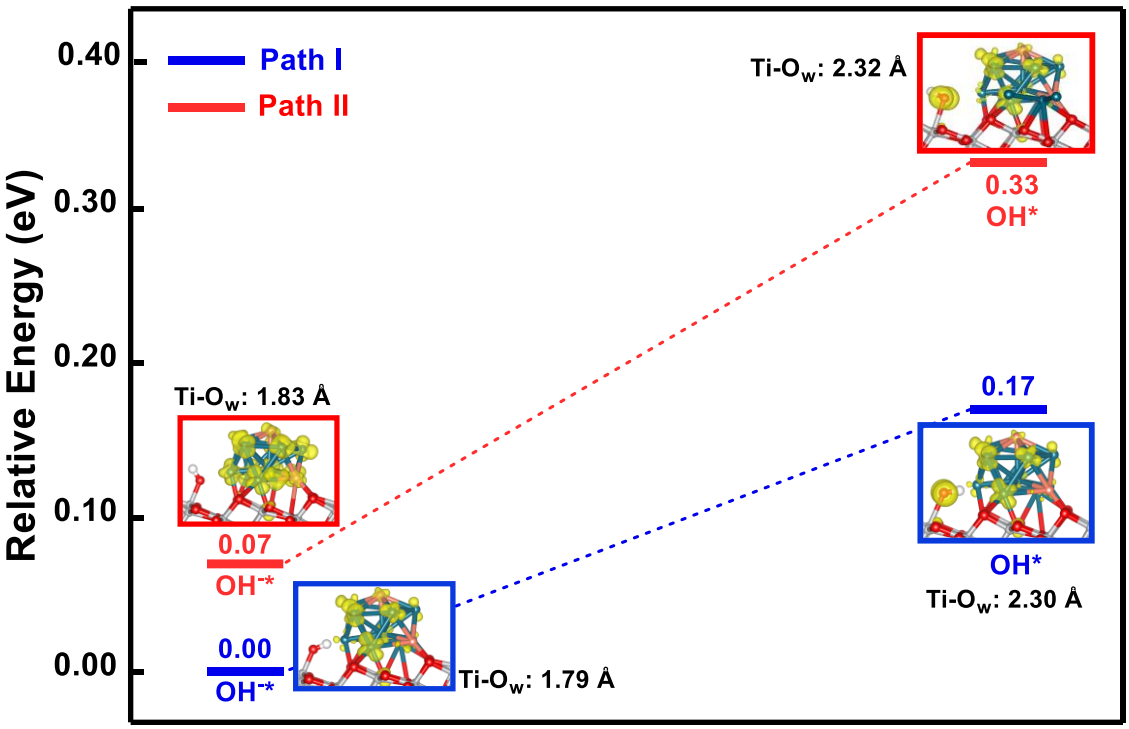

Figure S30. The process in which OH^- combines with a hole to form OH is endothermic (~0.2 eV), and the hole transfer barrier is taken from the literature[8].

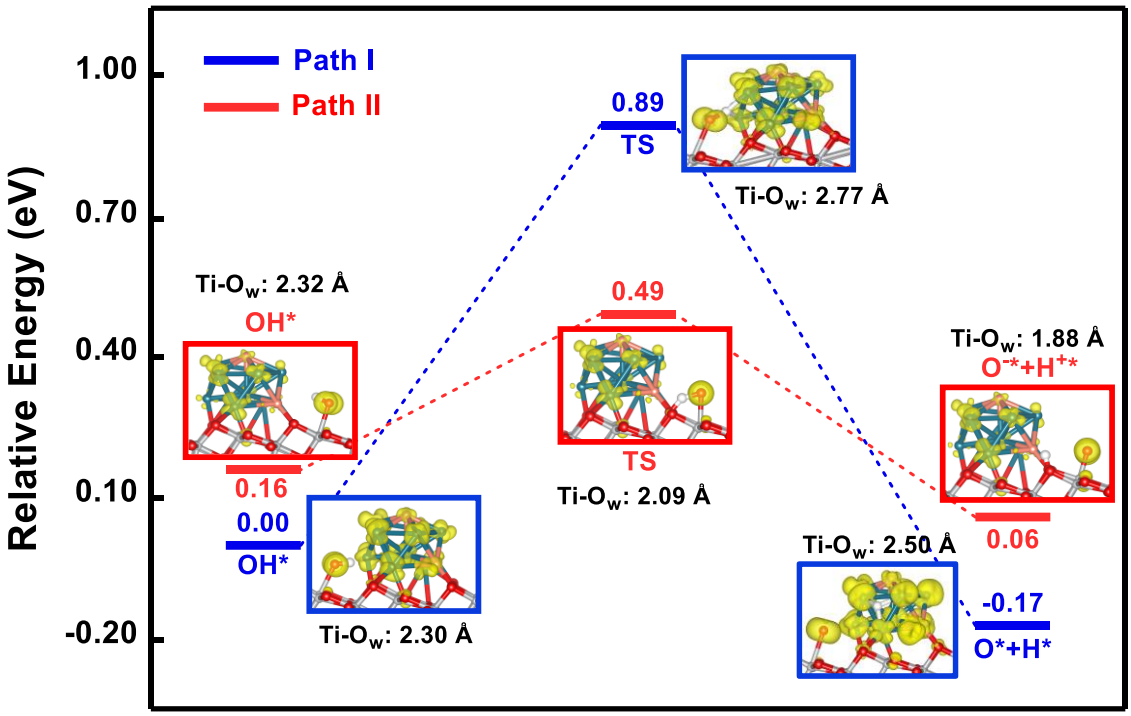

Figure S31. The reaction pathways for OH dissociation yielding O/H (path I) and O^-/H^+ (path II) with hole involvement. Reactions involving hole are more favorable both kinetically and thermodynamically compared to those without hole involvement.

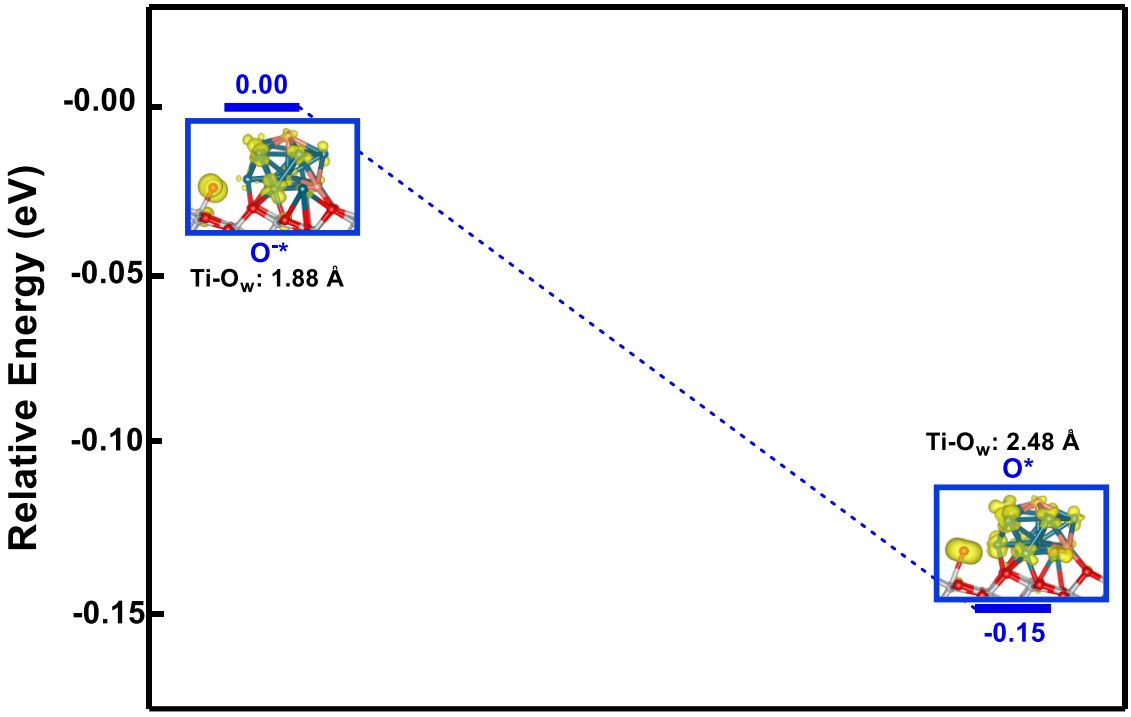

Figure S32. The process in which O^- combines with a hole to form O is exothermic (0.15 eV), and the hole transfer barrier is taken from the literature[8].

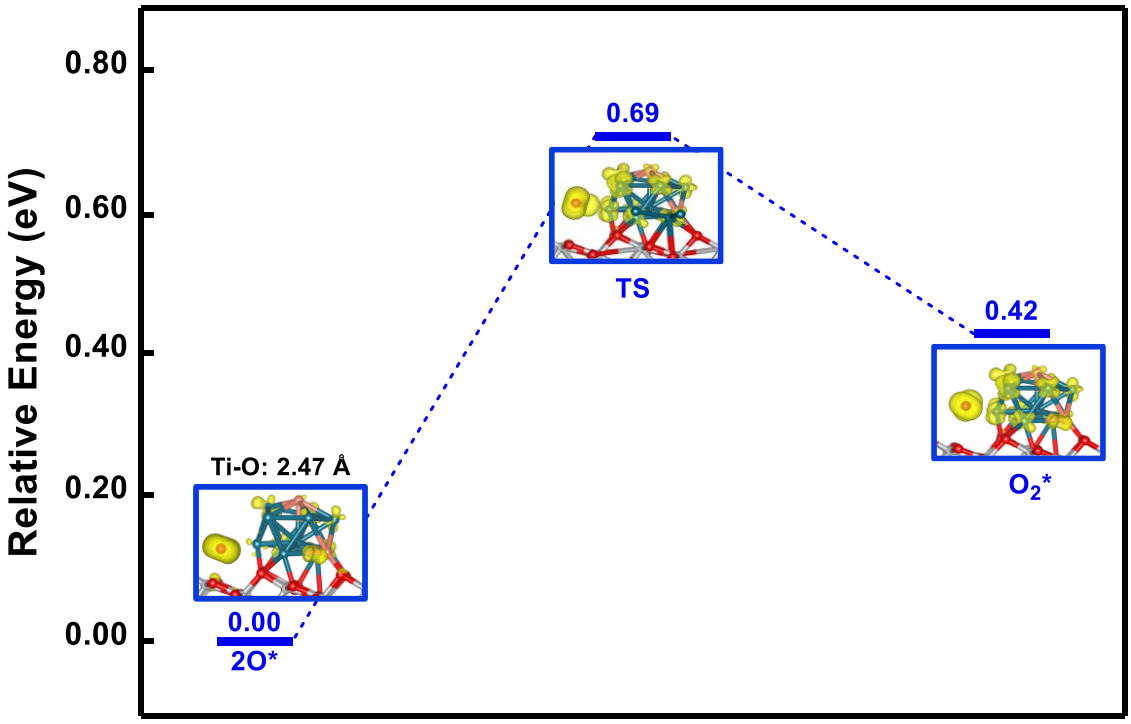

Figure S33. The reaction pathway for O_2 formation via forming a bond between two O atoms.

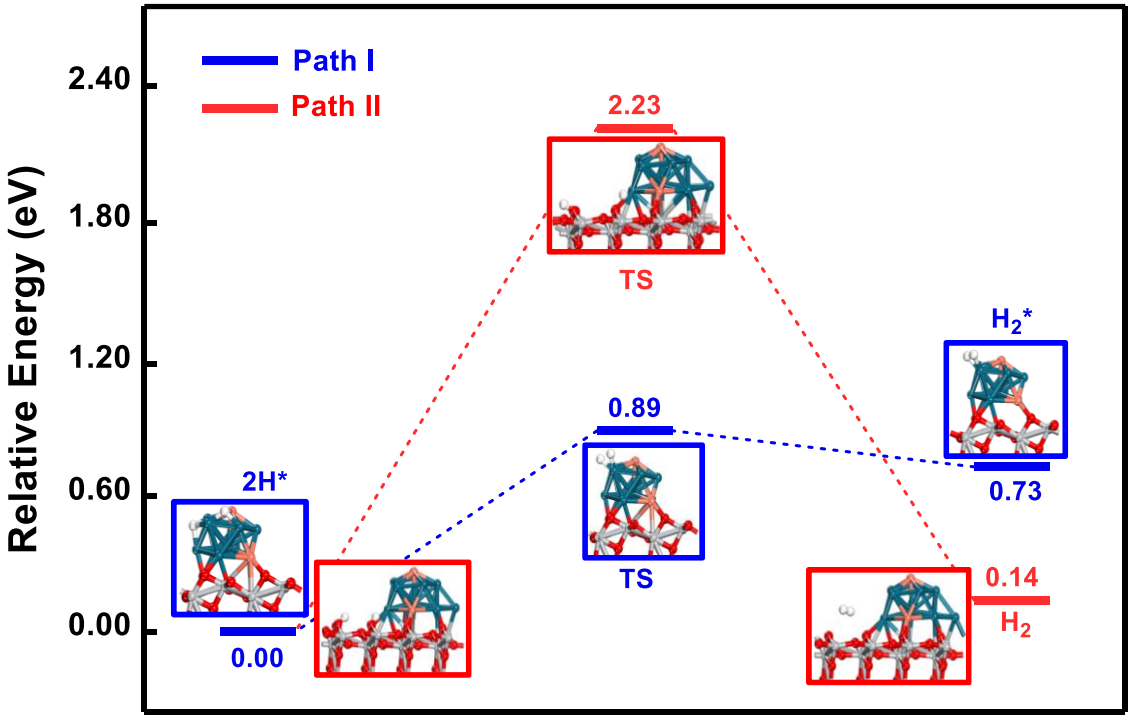

Figure S34. The reaction routes for H_2 formation from H (path I) and H^+ (path II) resulting from water dissociation.

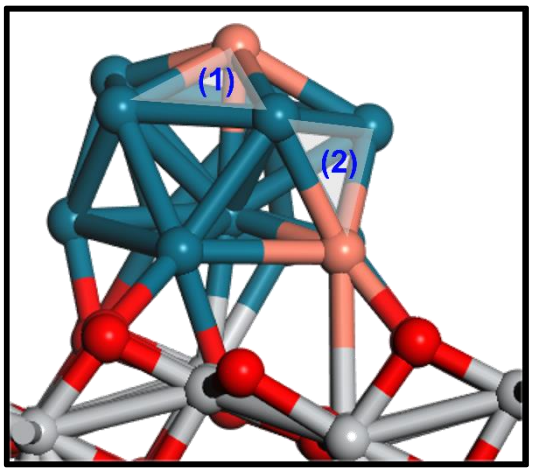

Figure S35. The two Pd_2Cu_1 adsorption sites. (1) adsorbs the H atom and (2) adsorbs the *CO molecule.

Tables

Table S1. HSE06 + D3 Calculated the Adsorption Energies of the $Pd_{11}Cu_2$ Clusters with Different Positions of Two Doped Cu atoms on the TiO_2(101) Surface.

Model	**ISO-1**	**ISO-2**	**ISO-3**	**ISO-4**			
E_{ads} (eV)	5.92	5.55	5.67	5.86			
Model	**NEI-1**	**NEI-2**	**NEI-3**	**NEI-4**	**NEI-5**	**NEI-6**	**NEI-7**
E_{ads} (eV)	5.92	5.62	5.86	5.83	5.30	5.48	5.51

Table S2. The -ICOHP Values and Enthalpy Changes of the *C*O <-> H*C*O Process Related to the Eleven Models of $Pd_{11}Cu_2$@TiO_2 as well as Selected Energy Barriers.

Model	**ISO-1**	**ISO-2**	**ISO-3**	**ISO-4**	**ISO-5**	**ISO-6**
-ICOHP (α/β)	1.64/1.76	2.20/2.24	2.19/2.17	3.04/4.32	2.22/2.71	3.47/3.49
ΔE (eV) (E_{H*C*O}-E_{*C*O})	-0.60	+0.67	-0.43	+0.47	+0.48	+0.45
E_{TS} (eV)	0.11	1.42	0.15	/		
Model	**ISO-7**	**ISO-8**	**NEI-1**	**NEI-2**	**NEI-3**	**NEI-4**
-ICOHP (α/β)	2.27/2.63	3.07/3.03	2.59/2.53	4.70/5.58	2.21/2.88	3.66/3.26
ΔE (eV) (E_{H*C*O}-E_{*C*O})	+1.23	+0.50	+0.16	+0.71	+0.21	+0.58
E_{TS} (eV)			0.32	1.21	0.39	/
Model	**NEI-5**	**NEI-6**	**NEI-7**	**NEI-8**		
-ICOHP (α/β)	4.09/5.00	1.66/2.24	2.76/3.01	1.95/2.23		
ΔE (eV) (E_{H*C*O}-E_{*C*O})	+0.71	+1.2	+1.04	+0.73		
E_{TS} (eV)	/	/	/			

Table S3. List about Reversibility (Z_i), Forward Reaction Rate Constants (k^+), Net Reaction Rates (r_{net}), Gibbs Free Energy Changes (ΔG), and Gibbs Energy Barriers (E_a) for all Elementary Reactions Considered in the Microkinetic Simulation. ΔG and E_a are Corrected with Entropy Effects and Zero-Point Energy (ZPE) Included. Adsorption or Desorption Process of Gas Molecule is Calculated with the Collision Theory (see Section I). #1, #2, #3, #4, #5 and #6 represent Ti_{5c}, O_{2b}, Pd_2Cu_1 (adsorbing H), interface, Pd_2Cu_1 (adsorbing *CO) and Pd_3 sites.

Step i		Z_i	k^+	r_{net}	ΔG	E_a
R1	$H_2O(l)+\#1<->H_2O\#1$	0.99	5.01e+08	4.05e-14	-0.71	-
R2	$H_2O\#1+\#2<->H^+\#2+OH^-\#1$	0.99	1.13e+03	2.06e-04	0.12	0.58
R3	$H_2O\#1+\#3<->H\#3+OH^-\#1+e^-$	1.0	2.45e+03	-2.06e-04	-0.06	0.56
R4	$OH^-\#1+h^+<->OH\#1$	0.99	2.49e+04	4.05e-14	0.17	0.50
R5	$OH\#1+\#3<->O\#1+H\#3$	6.55e-03	3.17e-04	9.64e-13	-0.34	0.97
R6	$OH\#1+\#2<->O^-\#1+H^+\#2$	1.0	2.58e+06	-9.24e-13	0.12	0.38
R7	$O^-\#1+h^+<->O\#1$	1.0	2.49e+04	-9.24e-13	-0.15	0.50
R8	$2O\#1<->O_2+2\#1$	1.11e-11	1.89e-04	2.02e-14	0.68	0.75
R9	$2H\#3<->H_2+2\#3$	1.22	1.03e-03	-2.24e-04	0.72	0.77
R10	$2H^+\#2+2e^-<->H_2+2\#2$	9.59e-14	2.50e-17	1.12e-17	-0.42	1.75
R11	$CO_2+\#4<->CO_2\#4$	3.68e-03	9.56e+08	3.69e-05	-1.08	-
R12	$CO_2\#4+H^+\#2+e^-<->OCHO\#4+\#2$	3.44e+05	4.84e-02	-1.81e-05	0.18	0.84
R13	$OCHO\#4+H^+\#2+e^-<->HCOOH\#4+\#2$	1.0	2.83e+11	-1.81e-05	-0.04	0.08
R14	$HCOOH\#4<->HCOOH(l)+\#4$	8.86e+12	1.99e-13	-1.81e-05	1.29	-
R15	$CO_2\#4 + H\#2 <->OCOH\#4+\#2$	0.99	2.88e+12	5.51e-05	-0.04	0.02
R16	$CO_2\#4 + \#5 <-> CO\#5 + O\#4$	1.88e+14	2.23e-02	-2.39e-24	-0.66	0.86
R17	$O\#4+H\_p\#2+e^-<-> OH\#4 + \#2$	1.00	9.04e+11	-2.39e-24	-0.48	0.05
R18	$CO\#5<->CO(g)+\#5$	6.59e+11	3.62e-36	-2.39e-24	2.65	-
R19	$OCOH\#4+H\#2<->CO\#4+H_2O+\#2$	1.48e-22	5.30e+03	5.51e-05	-0.99	0.54
R20	$CO\#4+H\#3<->HCO\#4+\#3$	4.49 e-01	2.78e+10	5.51e-05	-0.6	0.14
R21	$CO\#4+ H\#2<->COH\#4+\#2$	1.22e+15	1.86e-12	-5.44e-12	1.22	1.46
R22	$COH\#4 + H\#3<->HCOH\#4+ \#3$	2.50e+05	7.66e+02	-5.44e-12	-0.03	0.59
R23	$HCO\#4 + H\#2<->HCOH\#4 + \#2$	0.99	1.13e+03	5.51e-05	0.55	0.58
R24	$HCO\#4 + H\#3<->CH_2O\#4 + \#3$	0.99	2.23e-02	1.54e-14	0.70	0.86
R25	$HCOH\#4+H\#3<->CH_2OH\#4+\#3$	1.69e+02	3.54e+02	-2.89e-06	0.31	0.61
R26	$HCOH\#4+\#6<->CH\#6+OH\#4$	4.22e-10	1.19e+06	5.79e-05	-0.78	0.40
R27	$CH_2O\#4+H\#2<->CH_2OH\#4+\#2$	3.73e+03	3.29e-23	-1.28e-29	0.24	2.10
R28	$CH_2O\#4+H\#3<->CH_3O\#4+\#3$	4.77e-04	9.92e-05	1.54e-14	0.40	1.00
R29	$CH_3O\#4+H\#2<->CH_3OH\#4+\#2$	1.13e-02	7.66e+02	1.54e-14	-0.46	0.59
R30	$OH\#4 + H\#2<->H_2O\#4+\#2$	0.99	1.33e+12	7.68e-05	-0.13	0.04

R31	H_2O#4<->H_2O(l)+#4	0.95	1.77e-03	7.68e-05	0.71	-
R32	CH#6+H#3<->CH_2#6 + #3	0.91	7.39e+00	5.79e-05	0.46	0.71
R33	CH_2OH#4+#3<->CH_2#6+OH#4	2.07e-17	1.72e+05	1.88e-05	-0.93	0.45
R34	CH_2#6+H#3<->CH_3#6+#3	1.91e-04	2.49e+04	7.68e-05	0.14	0.50
R35	CH_3#6+H#3<->CH_4+#3+#6	0.99	4.25e+12	7.68e-05	-0.22	0.01
R36	CH_2OH#4+H#3<->CH_3OH#4+#3	5.63e+02	3.54e+02	-2.17e-05	0.39	0.61
R37	CH_3OH#4<->CH_3OH(l)+#4	1.11e+17	5.28e-12	-2.17e-05	1.04	-
R38	CH_3OH#4+#6<->CH_3#6+OH#4	1.24e-13	3.17e-04	1.18e-14	-0.57	0.97

Table S4. Computed Coverages of Surface Species at #1, #2, #3, #4, #5, and #6.

#1 (Ti_{5c} site)					
H_2O	**O**	**OH**	**OH^-**	**O^-**	**#1**
0.99	1.03e-05	6.58e-06	4.72e-03	3.12e-08	2.12e-14

#2 (O_{2b} site)	
H^+	**#2**
0.67	0.33

#3 (Pd_2Cu_1 site)	
H	**#3**
0.99	4.66e-04

#4 (interface site)					
CH_2O	**CH_2OH**	**CH_3O**	**CH_3OH**	**HCOOH**	**CO**
1.55e-10	1.09e-10	3.03e-17	3.71e-11	1.03e-05	3.59e-15
CO_2	**COH**	**H_2O**	**HCO**	**HCOH**	**O**
1.62e-09	2.84e-20	0.96	4.15e-02	4.86e-11	1.31e-11
OCHO	**OCOH**	**OH**	**#4**		
1.08e-06	1.55e-08	3.08e-03	1.94e-14		

#5 (Pd_2Cu_1 site)	
CO	**#5**
1	0

#6 (Pd_3 site)			
CH	**CH_2**	**CH_3**	**#6**
8.46e-05	3.08e-09	5.63e-12	0.99

Table S5. Reaction Rates of R14 and R37 at Different Concentrations (mol/L) of HCOOH and CH_3OH, along with X_{RC} of Key Steps.

R14: HCOOH#4<->HCOOH(l)+#4	**R37: CH_3OH#4<->CH_3OH(l)+#4**	**Key Rate Steps**	X_{RC}
C_{HCOOH} = 10, C_{CH3OH} = 10			
-1.32e-04	-1.58e-04	HCOOH#4<->HCOOH(c)+#4 HCOH#4+#6<->CH#6+OH#4 H_2O#4<->H_2O(c)+#4 CH_3OH#4<->CH_3OH(c)+#4	0.22 0.15 0.17 0.39
C_{HCOOH} = 1, C_{CH3OH} = 1			
-1.81e-05	-2.17e-05	CO_2+#4<->CO_2#4 HCOOH#4<->HCOOH(c)+#4 CH_3OH#4<->CH_3OH(c)+#4	0.43 0.21 0.27
C_{HCOOH} = 0.1, C_{CH3OH} = 0.1			
-1.88e-06	-2.25e-06	CO_2+#4<->CO_2#4 HCOOH#4<->HCOOH(c)+#4 CH_3OH#4<->CH_3OH(c)+#4	0.85 0.04 0.05
C_{HCOOH} = 0.01, C_{CH3OH} = 0.01			
-1.88e-07	-2.26e-07	CO_2+#4<->CO_2#4	0.94
C_{HCOOH} = 0.001, C_{CH3OH} = 0.001			
-1.88e-08	-2.26e-08	CO_2+#4<->CO_2#4	0.95

Table S6. Key Radicals Involved in Photocatalytic Splitting of Water, Including Bader Charges, Distances to Ti, and Magnetic Moments.

Radicals	**Bader Charge (e-)**	**Ti-O (Å)**	**Magnetic moment**
OH	7.05 (6.7[O]+0.35[H])	2.30	0.81
OH^-	7.54 (7.23[O]+0.31[H])	1.79	0
O	6.03	2.48	1.62
O^-	6.58	1.89	0.89
O^{2-}	6.93	1.69	0.08

References

1. Dumesic, J. A. Analyses of Reaction Schemes Using De Donder Relations. *J. Catal.* **1999**, *185,* 496-505.
2. Campbell, C. T. The Degree of Rate Control: A Powerful Tool for Catalysis Research. *ACS Catal.* **2017**, *7,* 2770-2779.
3. Stegelmann, C.; Andreasen, A.; Campbell, C. T. Degree of Rate Control: How Much the Energies of Intermediates and Transition States Control Rates. *J. Am. Chem. Soc.* **2009**, *131,* 8077-8082.
4. Long, R.; Li, Y.; Liu, Y.; Chen, S.; Zheng, X.; Gao, C.; He, C.; Chen, N.; Qi, Z.; Song, L.; Jiang, J.; Zhu, J.; Xiong, Y. Isolation of Cu Atoms in Pd Lattice: Forming Highly Selective Sites for Photocatalytic Conversion of CO_2 to CH_4. *J. Am. Chem. Soc.* **2017**, *139,* 4486-4492.
5. Ren, G.; Zhou, M.; Wang, H. Weakened Interfacial Hydrogen Bond Connectivity Drives Selective Photocatalytic Water Oxidation toward H_2O_2 at Water/Brookite-TiO_2 Interface. *J. Am. Chem. Soc.* **2024**, *146,* 6084-6093.
6. Wang, D.; Sheng, T.; Chen, J.; Wang, H.-F.; Hu, P. Identifying the Key Obstacle in Photocatalytic Oxygen Evolution on Rutile TiO_2. *Nat. Catal.* **2018**, *1,* 291-299.
7. Wang, D.; Wang, H. F.; Hu, P. Identifying the Distinct Features of Geometric Structures for Hole Trapping to Generate Radicals on Rutile TiO_2(110) in Photooxidation Using Density Functional Theory Calculations with Hybrid Functional. *Phys. Chem. Chem. Phys.* **2015**, *17,* 1549-1555.
8. Deskins, N. A.; Dupuis, M. Intrinsic Hole Migration Rates in TiO_2 from Density Functional Theory. *J. Phys. Chem. C* **2009**, *113,* 346-358.